Materials Today Bio 37 (2026) 103019

Contents lists available at ScienceDirect

Materials Today Bio

journal homepage: www.journals.elsevier.com/materials-today-bio

Copper-doped β-tricalcium phosphate: synthesis, characterization, and *in vitro* osteoclastic resorption

Bastien Le Gars Santoni [a,b], Nicola Döbelin [a], Silvia Dolder [c], Roman Heuberger [a], Yassine Maazouz [a], Christoph Stähli [a], Paul Bowen [d], Willy Hofstetter [c], Marc Bohner [a,*]

[a] RMS Foundation, Robert Mathys Strasse 1, Bettlach, CH-2544, Switzerland
[b] Graduate School for Cellular and Biomedical Sciences, University of Bern, Bern, CH-3012, Switzerland
[c] Bone & Joint Program, Department for BioMedical Research (DBMR), University of Bern, Murtenstrasse 35, Bern, CH-3008, Switzerland
[d] EPFL, Ecole Polytechnique Fédérale de Lausanne, Laboratory of Construction Materials, Station 12, Lausanne, CH-1015, Switzerland

ARTICLE INFO

Keywords:
β-tricalcium phosphate
Copper doping
Grain boundaries
Osteoclasts
Resorption
Biomaterials

ABSTRACT

This study investigated how copper (Cu) incorporation and grain-boundary segregation in β-tricalcium phosphate (β-TCP) influence microstructure, surface chemistry, and *in vitro* osteoclastic resorption. β-TCP powders containing 0–2.4 wt% Cu were synthesized via precipitation of Cu-substituted calcium-deficient hydroxyapatite (CDHA) followed by thermal conversion. Phase composition, chemistry, and microstructure were characterized using X-ray diffraction (XRD), inductively coupled plasma mass spectrometry (ICP-MS), scanning electron microscopy (SEM), and X-ray photoelectron spectroscopy (XPS). Dense β-TCP cylinders were fabricated, polished, and incubated with primary murine osteoclasts. Osteoclastic resorption was quantified by white-light interferometry (WLI) and ion release analysis. Cu incorporation in CDHA and β-TCP increased proportionally with the Cu concentration in the precipitation solution. At low concentrations, Cu substituted for Ca at the Ca(5) site in the β-TCP lattice, whereas at higher Cu contents, CuO segregated at grain boundaries. Tartrate-resistant acid phosphatase (TRAP) positive osteoclasts were observed on all samples; however, Cu content strongly modulated resorptive activity. β-TCP containing 0.1 wt% Cu exhibited deeper and more localized resorption pits, indicating enhanced localized osteoclastic activity. In contrast, higher Cu levels progressively reduced resorption, with complete inhibition observed at 2.4 wt% Cu. These results identify an optimal Cu doping level near 0.1 wt%. While grain-boundary segregation of Cu as CuO was confirmed at higher doping levels, its specific contribution to the biological response could not be resolved in this study.

1. Introduction

Bone defects that exceed a critical size require the support of bone graft substitutes to enable proper regeneration [1]. While autologous bone remains the gold standard, its limited availability and complication rates of iliac crest bone harvesting close to 20% [2–4] have led to increasing reliance on synthetic alternatives. Among these, calcium phosphate (CaP) ceramics such as hydroxyapatite (HA; $Ca_5(PO_4)_3OH$), β-tricalcium phosphate (β-TCP; β-$Ca_3(PO_4)_2$), and their composites have garnered significant attention due to their chemical similarity to bone mineral, biocompatibility, and tunable resorption properties [5,6].

Among CaP ceramics, β-TCP is particularly notable for its cell-mediated resorption [7–9], which allows a graft substitute to be progressively replaced by newly formed bone at a rate compatible with the host's metabolism. Resorption typically begins at grain boundaries [10,11], suggesting that these regions are chemically less stable than the bulk material. Kalita and Bhatt [12] further demonstrated that doping HA with zinc (Zn) and magnesium (Mg) accelerates its degradation in simulated body fluid (SBF). Given that undoped HA is generally insoluble in SBF, this implies that grain boundaries, particularly those modified by Zn and Mg doping, are more prone to dissolution under physiological conditions. However, doping does not universally promote degradation; for instance, Mg-doping has been shown to stabilize grain boundaries in β-TCP [13], indicating that the effect of dopants can vary depending on the material and context.

The mechanisms by which dopants influence grain boundary stability and, consequently, the *in vitro* and in vivo behavior of the material remain poorly understood. A major challenge is the difficulty of

* Corresponding author.
E-mail address: marc.bohner@rms-foundation.ch (M. Bohner).

https://doi.org/10.1016/j.mtbio.2026.103019
Received 27 December 2025; Received in revised form 9 March 2026; Accepted 9 March 2026
Available online 11 March 2026
2590-0064/© 2026 The Authors. Published by Elsevier Ltd. This is an open access article under the CC BY-NC license (http://creativecommons.org/licenses/by-nc/4.0/).

accurately characterizing the chemical composition of grain boundaries. Solid-state nuclear magnetic resonance can provide indirect insights into the chemical species present at these interfaces [14], but it lacks spatial resolution. Atom probe tomography, while capable of delivering high-resolution compositional data, is technically challenging to apply to ceramics and particularly to CaP due to their insulating nature and structural fragility [15]. Analysis is further complicated by the possible presence of distinct grain boundary phases, known as complexions, which may obscure or confound interpretation [16]. Moreover, since grain boundaries constitute only a small fraction of the total material volume, even trace amounts of dopants can significantly alter their composition, potentially leading to substantial changes in biological performance.

Copper (Cu) ions are well known for their antimicrobial and antibacterial properties, largely due to their inherent cytotoxicity [17–20]. At the same time, Cu is an essential trace element that plays multiple vital roles in human physiology [21]. It is involved in iron metabolism [22,23], defense against reactive oxygen species (ROS) via Cu-dependent enzymes [24–26], and the enzymatic crosslinking of collagen and elastin through lysyl oxidase (LOX) [27]. Cu also contributes to angiogenesis [28], endothelial cell development [29], and the differentiation of mesenchymal stem cells into osteoblasts [30]. Accordingly, Cu deficiency has been linked to bone loss [31] and cardiovascular abnormalities [32]. Furthermore, low concentrations of Cu (0-8 μM) have been shown to reduce osteoclast viability and resorption activity [33]. Excessive Cu levels are harmful; in genetic disorders such as Wilson's disease, Cu accumulation in organs like the liver and brain can cause neurological and hepatic dysfunction [26,34].

Due to these multifunctional roles, Cu ions have been incorporated into bioglasses [35–37] and CaP ceramics [28,38–41] to improve their biological performance. Despite ISO standard 13175-3 limiting the heavy metal content (including Cu) in commercial CaP to 50 ppm among total heavy metals, experimental studies often exceed this limit by several orders of magnitude to investigate the effects of Cu across a broader concentration range. In β-TCP, Cu is primarily substituted at Ca (5) sites in the crystal lattice, with incorporation levels reported up to 15 mol% [42,43]. Owing to its smaller ionic radius compared to Ca, Cu substitution leads to a decrease in lattice parameters and unit cell volume [42,43]. While Cu has generally been associated with enhanced osteoblast differentiation [30], Yang et al. observed a reduction in alkaline phosphatase activity, a marker of osteoblastic function, along with significant inhibition of osteoclast development and activity [41], findings consistent with those of Wilson et al. using $CuSO_4$ [44]. More recently, Gomes et al. demonstrated good biocompatibility and cell adhesion on Cu-doped biphasic CaP (BCP) disks [40].

Despite these findings, the mechanisms underlying Cu's biological effects in Cu-doped CaP remain unclear. It is not yet established whether these effects result from Cu ion release into the cell culture medium or from uptake during resorption of Cu-rich particles or surfaces. Additionally, it is unknown whether Cu segregates at β-TCP grain boundaries, which could influence both its release kinetics and biological behavior. In other words, the role of Cu segregation at β-TCP grain boundaries in controlling osteoclastic resorption has not yet been elucidated. In fact, there is to the best of our knowledge no *in vitro* study looking at the effect of Cu-doping on β-TCP osteoclastic resorption.

This study is based on the hypothesis that Cu segregation at the grain boundaries of Cu-doped β-TCP plays a key role in mediating its biological response. Accordingly, the aim of this work was to systematically investigate how increasing Cu doping levels affect the physicochemical properties of β-TCP, especially grain-boundary chemistry and microstructure, and to determine how these changes translate into alterations in osteoclast-mediated resorption. To address this, five β-TCP compositions containing Cu concentrations ranging from 0.0 wt% to 2.4 wt% were synthesized, with three independent batches prepared for each composition. The powders were characterized using a suite of standard techniques, including nitrogen adsorption (BET method), powder X-ray diffraction (XRD), inductively coupled plasma mass spectrometry (ICP-MS), and scanning electron microscopy (SEM). Dense cylindrical samples were then fabricated from the Cu-doped powders to assess the influence of Cu incorporation on physical properties such as grain size, density, and surface chemistry (using X-ray photoelectron spectroscopy (XPS)), as well as on osteoclastic resorption behavior. Resorption was evaluated using both physical measurements via white-light interferometry (WLI) and chemical analysis through ICP-MS.

2. Materials and methods

Powder synthesis: Cu-doped β-TCP powders were produced by thermal conversion of Cu-doped CDHA. The approach was similar to the one used for the production of pure CDHA/β-TCP [45,46]. Cu-doped CDHA was synthesized via an aqueous precipitation method [47,48]. Specifically, 250 mL of a 0.6 M diammonium hydrogen phosphate ($(NH_4)_2HPO_4$) solution (Art N°5596.1, Batch N°138269744, Carl Roth) were added dropwise at 4 mL/min into 250 mL of a 0.9 M Ca and Cu nitrate solution. The required amount of $Cu(NO_3)_2{\cdot}xH_2O$ (Art N°229636, Batch N°MKCC0069, Sigma-Aldrich, Switzerland; assumed to be anhydrous) was dissolved together with $Ca(NO_3)_2{\cdot}4H_2O$ (Art N°102123, Batch N°B1371623, Merck) to yield a precursor solution with a [Ca + Cu]/P molar ratio of 1.500 (Table 1). Ratios below 1.50 were classified as "low", whereas ratios above 1.50 were classified as "high". During the synthesis, pH was maintained at 8.0 by compensating for the drop in pH using a 32 % ammonia solution (NH_4OH; Art. No. 338818, Batch No. SZBF3200 V, Sigma-Aldrich) [49]. A pH value of 8.0 was selected based on a previous study on the synthesis of chemically pure β-TCP powders [46]. That study demonstrated that pH 8.0 provides optimal conditions for stabilizing the β-TCP phase while minimizing the formation of secondary phases (β-CPP and HA). Specifically, lower pH values led to increased β-CPP formation, whereas more alkaline conditions promoted the formation of HA as a secondary phase due to the higher availability of hydroxyl ions. Following complete addition of the phosphate solution, the reaction mixture was allowed to ripen under continuous stirring for 48 h at 30 °C [49]. The resulting CDHA precipitate was filtered, rinsed with deionized water, dried at 70 °C for 24 h, manually ground using a mortar, and sieved to obtain particles <500 μm. Finally, CDHA was converted into β-TCP via calcination at 850 °C for 1 h.

The Cu doping levels were selected following a stepwise experimental approach rather than a uniformly spaced compositional series. Low Cu contents (0.1 and 0.5 wt%) were used to confirm Cu incorporation into β-TCP while maintaining phase purity, whereas a higher nominal Cu content (2.4 wt%) was targeted to approach the upper limit of Cu incorporation and assess possible excess Cu effects. An intermediate composition (1.4 wt%) was obtained experimentally to bridge the low- and high-doping regimes.

Polished cylinder synthesis: The preparation of β-TCP cylinders followed procedures previously described [11,49,50]. β-TCP powders were first ball-milled in an aqueous medium for 2 h to eliminate agglomerates formed during the calcination process. The powders were then filtered, dried at 70 °C, and dispersed in a 1.0 wt% solution of Darvan C-N (ammonium polymethacrylate; R.T. Vanderbilt Co., USA). The resulting slurries were further homogenized by ball-milling for 30 min before being slip-cast into modified 96-well polystyrene plates (the bottom part was cut off; Art. No. 3628, Batch No. 16117017, Costar®, Corning Incorporated, USA), which were placed on gypsum blocks to facilitate drying. After drying and demolding, dense β-TCP cylinders were obtained by sintering the green bodies at 1100 °C for 3 h. Importantly, the green bodies were placed on stabilized zirconia plates (Composition 1661, Art. N°S-3406-0.25, Batch N° 08021504, Zircoa, USA) previously coated with the same β-TCP powder as the one used for the manufacture of the cylinders, to avoid any chemical contaminations from the zirconia plate and sample cracking due to differences of thermal expansion with the plate. One face of each cylinder was then sequentially ground using

Table 1
Main synthesis parameters of pure and Cu-doped CDHA/β-TCP powders. For the calculation of the (Ca + Cu)/P ratio, it was assumed that x = 0 in the copper nitrate composition, leading to a molecular weight for $Cu(NO_3)_{2\cdot xH2O\ of}$ Mw = 187.56 g/mol. The Cu nominal content is the Cu/(Ca + Cu) mol% ratio. The samples are denominated in the text with their ICP-MS Cu weight fraction.

Cu nominal content [wt %]	Cu nominal content [mol %]	Sample denomination	$Ca(NO_3)_{2\cdot 4H2O}$ [g]	$Cu(NO_3)_{2\cdot xH2O}$ [g]	$(NH_4)_2HPO_4$ [g]	[Ca + Cu]/P [−]	Synthesis pH [−]
0.00	0.00	0.0%	53.13	0.000	19.81	1.500	8.00
0.06	0.10	0.1%	53.08	0.042	19.81	1.500	8.00
0.61	1.00	0.5%	52.60	0.422	19.81	1.500	8.00
1.78	2.92	1.4%	51.59	1.232	19.81	1.500	8.00
3.04	5.00	2.4%	50.48	2.110	19.81	1.500	8.00

silicon carbide (SiC) abrasive papers, followed by polishing with diamond suspensions (down to 0.25 μm) and a final polishing using a 0.2 μm silica suspension. To ensure cleanliness, the polished β-TCP cylinders were ultrasonically cleaned in acetone (2 × 5 min) and ethanol (1 × 5 min).

XRD: β-TCP powders were characterized by XRD using a Bruker D8 Advance diffractometer (Bruker AXS GmbH, Germany). The general procedure was already described in Ref. [46]. For XRD analysis, β-TCP powders were dwelled at 1000 °C for 15 h followed by 15 h at 840 °C [51]. XRD patterns were collected using digitally and Ni-filtered Cu Kα radiation (λ = 1.540598 Å) and analyzed via Rietveld refinement with Profex (Version 4.0.2) [52]. Scans were performed from 8° to 100° (2θ). The JCPDS file numbers for HA, β-TCP, and β-CPP used for the Rietveld refinement analysis are 01-074-0565, 04-008-8714, and 04-009-3876, respectively.

ICP-MS: The elemental impurity content in β-TCP powders was determined using ICP-MS (Agilent 7700x, Agilent Technologies, USA) equipped with an autosampler (SPS 4, Agilent Technologies, USA), following the methodology previously described [46,49]. Samples were first digested in concentrated nitric acid (HNO_3, 69% w/w, ROTIPURAN® Supra, Art. N° HN50.1, Roth, Germany), then diluted 1:100 in an acidic matrix solution composed of ultrapure water containing 3% HNO_3, 2% hydrochloric acid (HCl, 35% w/w, ROTIPURAN® Supra, Art. N° HN53.1, Roth, Germany), and 0.01% hydrofluoric acid (HF, 47–51% w/w, UPATM, Art. N° SS52, Romil, UK). Ca and P concentrations were determined by calibrating ^{44}Ca and ^{31}P signals using a custom-made Ca/P standard solution (500:250 ppm Ca:P, Inorganic Ventures, serially diluted to 5000:2500, 1000:500, 200:100, and 40:20 ppb). ^{23}Na, ^{88}Sr, ^{24}Mg, and ^{65}Cu signals were calibrated using a certified multi-element standard (71A, 10 ppm, Inorganic Ventures, diluted to 100, 10, 1, and 0.1 ppb). An internal standard (1 ppb In, 1 ppb Sc, and 0.1 ppb Bi, Inorganic Ventures) was included with each sample to correct for matrix effects and instrumental drifts. Additionally, the Ca/P and 71A standards were measured after every 8 samples to compensate for mass-dependent calibration drifts over time. Measurement uncertainties ($U_{k\ =\ 2}$) were calculated for each element based on a three-day validation protocol, accounting for pipetting errors, weighing inaccuracies, and instrument variability. ICP-MS analysis was also performed on the cell culture medium, which was diluted 1:1000 in the same acidic matrix. Calibration of ^{44}Ca and ^{31}P was again done using the Ca/P standard (diluted to 5000:2500, 500:250, 100:50, 20:10, and 4:2 ppb). Other elements were calibrated with the 71A standard, as previously described. Calibration drifts were corrected using the same internal standards and repeated measurements of Ca/P and 71A.

Specific surface area (SSA): The SSA of CDHA and β-TCP powders was determined by nitrogen (N_2) adsorption at 77 K using a TriStar II Plus analyzer (Micromeritics, USA). The Brunauer–Emmett–Teller (BET) model was applied using five-point measurements to calculate the total surface area, from which SSA was derived. As moisture can significantly influence SSA measurements, samples were pre-dried for 3 h at 130 °C under a constant nitrogen flow using a FlowPrep 060 station (Micromeritics, USA). To ensure reliable data, a target surface area of approximately 10 m^2 was aimed for. Accordingly, 0.5 g of CDHA powder and 1.5 g of β-TCP were typically used per measurement. In addition, the diameter of the elementary particles (assumed spherical) was estimated from the specific surface area measurement using the equation d = 6/(SSA • ρ) [μm], where d is the diameter and ρ the density.

SEM: CDHA and β-TCP powders were examined using a field emission SEM (FE-SEM; Merlin, Zeiss, Germany) equipped with a high-efficiency secondary electron (HE-SE2) detector. Imaging was conducted at an accelerating voltage of 1 kV, with a probe current of 80 pA and a working distance of 4.0 mm [46]. For sample preparation, powders were mounted on carbon adhesive tape previously affixed to standard aluminum SEM stubs. To minimize charging effects and enable high-magnification imaging, CDHA powders were coated with a thin layer of osmium. In contrast, β-TCP powders were observed without coating. Similarly, the surfaces of β-TCP cylinders, both before and after cell culture experiments, were examined employing the same imaging parameters used for powder analysis. Specifically, the cylinders were mounted on standard aluminum SEM stubs using carbon adhesive tape and coated with a thin layer of carbon.

Grain size: Grain sizes were determined by morphometric analysis of backscattered electron (BSE) SEM images using the line intercept method. In this approach, straight lines were randomly drawn on the micrographs, and the number of intersections with grain boundaries was counted. The mean grain size (D) was calculated by dividing the total line length (L) by the number of intersections minus one (P − 1). This correction accounts for the fact that both ends of the line typically touch grain boundaries, meaning that the number of actual grains intersected is (P − 1). To ensure statistical robustness, grain size was measured on a large dataset: three cylinders were analyzed for each β-TCP batch, with three SEM images acquired per cylinder. On each image, approximately 100 grains were evaluated, yielding a total of 300 grains measured per cylinder/batch and hence 900 grains for each Cu composition.

Relative density: The relative density of the β-TCP cylinders was determined using the Archimedes' method. Initially, cylinders were degassed in an impregnation device (CitoVac, Struers, Denmark) and weighed dry (m_{dry}) using a high-precision scale. Subsequently, the samples were again degassed and impregnated with isopropanol in a beaker to facilitate penetration into open porosity. Density measurements were performed using a density determination kit (Mettler Toledo, Switzerland) installed on the scale. The beaker in which the sample was immersed was filled with isopropanol and tared before measurement. Cylinders were removed from the beaker with tweezers, gently rolled on a filter paper pre-moistened with isopropanol to remove surface excess and then placed in the isopropanol-immersed metal holder. After 30 s, the submerged mass (m_{wet}) was recorded. Timing during these steps was carefully controlled to ensure reproducibility despite isopropanol's volatility. The apparent density (ρ) of each cylinder was calculated using equation [1] and then expressed as a percentage relative to the theoretical density of β-TCP, determined from X-ray diffraction data. For accuracy, m_{wet} was measured 4–5 times per cylinder, and three cylinders were analyzed per batch. The density of isopropanol, ρ_{iso}, was adjusted based on its temperature during measurement, monitored with a Pt100 probe (Art. N° 00724, mcs Laboratory AG, Switzerland) and a calibrated thermometer (testo 735, Testo,

Switzerland).

$$\rho = \frac{m_{dry} \cdot \rho_{iso}}{m_{dry} - m_{wet}} \quad [1]$$

XPS: XPS measurements were performed using an Axis Nova spectrometer (Kratos Analytical Ltd., UK), equipped with a monochromatic Al Kα X-ray source (1486.7 eV), operated at 225 W and an incidence angle of 54.6° relative to the sample surface. The acquired spectra were processed using CasaXPS software (v2.3.14, Casa Software Ltd., UK). Peak fitting was conducted for the core-level signals of O 1s, C 1s, Ca 2p, and P 2p to accurately determine their binding energies. Charge correction was applied by referencing the C 1s peak of aliphatic carbon to 285.0 eV. Peak areas were calculated after background subtraction and corrected using relative sensitivity factors provided by the manufacturer.

Cell culture: Osteoclasts were generated from primary cells according to the procedure described by Gallo et al. [49] and Le Gars Santoni et al. [11]. Bone marrow cells (BMCs) were isolated from the femora and tibiae of 6-week-old C57Bl/6J mice and cultured for 24 h in α-minimum essential medium (α-MEM; Art. No. 12000, GIBCO® BRL Life Technologies, Switzerland), supplemented with 10% fetal bovine serum (FBS; Art. No. F7524, Batch No. 099K3395, Sigma-Aldrich, Switzerland), 1% penicillin/streptomycin (P/S; Art. No. 15140, GIBCO BRL Life Technologies, Switzerland), and 30 ng/mL macrophage colony-stimulating factor (M-CSF; Art. No. FDP-3005, Chiron, USA). After 24 h, the non-adherent osteoclast progenitor cells (OPCs) were collected and resuspended in fresh α-MEM supplemented with 30 ng/mL M-CSF and 20 ng/mL receptor activator of nuclear factor κ-B ligand (RANKL; recombinant human, Art. No. 310-01, PeproTech, UK). Mature osteoclasts were obtained after 5 days of differentiation. Meanwhile, β-TCP cylinders were sterilized via dry heat (180 °C for 6 h) and placed into 96-well plates with their polished surfaces facing upwards. Each cylinder was pre-conditioned by coating with 150 μL of 30% FBS in α-MEM and incubated for 48 h at 37 °C in a humidified atmosphere containing 5% CO_2. The coating medium was removed prior to seeding. On day 5, mature osteoclasts were seeded onto the β-TCP cylinders by adding 25 μL of cell suspension and 125 μL of medium supplemented with 30 ng/mL M-CSF, 15 mM HCl (37% fuming; Art. No. 317, Merck, Germany), and 20 ng/mL RANKL. As a control, macrophages were differentiated from OPCs in α-MEM supplemented with 30 ng/mL M-CSF but without RANKL.

Cell culture experiments were conducted in triplicate ($n = 3$) using three distinct β-TCP batches, each with a Ca/P molar ratio near 1.500 (Table 2). Each experiment involved incubating β-TCP cylinders for 24 h under three conditions: no cells (NC), macrophages (MA), or osteoclasts (OC). After 24 h of exposure to the cell culture medium, either with or without cells, the supernatants were collected, centrifuged (Eppendorf 5415R, 13,200 rpm, 16,100×*g*, 10 min), and stored in Eppendorf tubes for subsequent analysis by ICP-MS. Osteoclast differentiation was confirmed by staining for tartrate-resistant acid phosphatase (TRAP). Cells were washed with phosphate buffer solution (PBS), fixed in 4% paraformaldehyde (Art. No. 818715, Merck, Germany) in PBS, rinsed three times with deionized water, and stained using a commercial TRAP staining kit (Art. No. 387A, Sigma-Aldrich, Switzerland). TRAP activity was quantified in the resulting cell lysates by the enzymatic conversion of p-nitrophenyl phosphate (p-NPP; Art. No. N3254, Sigma, Switzerland) to p-nitrophenol in the presence of sodium tartrate and sodium acetate. The reaction was terminated with NaOH, and absorbance was measured at 405 nm (reference wavelength: 690 nm) using an Infinite 200Pro spectrophotometer (Tecan Group Ltd., Switzerland). The remaining cylinders were cleaned to remove cellular and medium residues. This was achieved by soaking the samples in a PBS-EDTA solution, followed by two rinses with distilled water (refreshed between steps), and finally drying them with isopropanol to prevent surface dissolution during storage. Factors, levels, responses and sample sizes of pure and Cu-doped β-TCP cylinders used in the cell-culture experiments are indicated in Table 3.

WLI: The surface topography of β-TCP cylinders was analyzed before and after cell culture experiments by WLI. Cylinders were examined using a non-contact 3D optical profiler (S neox, Sensofar, Spain) equipped with a 50 × WLI objective (50 × /0.55DI, CF Plan, Nikon, Japan). To expand the field of view to 665 μm × 501 μm, image stitching was performed using SensoSCAN software (Version 6.1.3, Sensofar, Spain). For each batch of β-TCP, three cylinders were analyzed, with three images acquired per cylinder. Image processing and surface characterization were conducted using SensoMAP Premium (Version April 7, 8341, Digital Surf, France). To define the baseline for analysis, a reference (zero) plane was manually selected by identifying non-resorbed surface areas. Roughness parameters according to ISO21920-3:2021, resorbed area, and resorbed volume per unit surface area were then calculated automatically by the software. The mean resorbed depth was derived by dividing the resorbed volume per surface area by the total resorbed area.

Table 3
Factors, levels, responses and sample sizes of pure and Cu-doped β-TCP cylinders used in the cell-culture experiments. Cylinders were produced with each of the 18 β-TCP powders.

Factor	Levels	Responses		
		TRAP Activity	Mean resorbed thickness	Cell culture medium (ICP-MS)
Cell culture medium with no cells (NC), with macrophages (MA) and with osteoclasts (OC)	3	$n = 3$	$n = 3$	$n = 3$
[Ca + Cu]/P molar ratio (bulk)	1 or 2[a]	$n = 18$	$n = 18$	$n = 18$
Cu content	5			

[a] For some Cu compositions, there was either at least one batch with a [Ca + Cu]/P molar ratio below 1.500 and one batch above 1.500 (number of levels = 2), while for other compositions all the batches had their [Ca + Cu]/P molar ratio below 1.500 (number of levels = 1).

Table 2
Factors, levels, responses and sample sizes analyzed for each batch of CDHA and β-TCP powders, as well as β-TCP cylinders. Powders were produced in triplicate except for the copper-free powders which were produced six times. As such, a total of 18 powders (1 x 6 + 4 x 3) were produced.

Factors			Levels	Responses			
				SSA	Grain Size	Relative density	XPS
powders	CDHA	[Ca + Cu]/P molar ratio (bulk)	1 or 2[a]	$n = 18$	-	-	-
		Cu content	5				
	β-TCP	[Ca + Cu]/P molar ratio (bulk)	1 or 2[a]	$n = 18$	-	-	-
		Cu content	5				
cylinders	β-TCP	[Ca + Cu]/P molar ratio (bulk)	1 or 2[a]	-	$n = 18$	$n = 18$	$n = 18$
		Cu content	5				

[a] For some Cu compositions, there was either at least one batch with a [Ca + Cu]/P molar ratio below 1.500 and one batch above 1.500 (number of levels = 2), while for other compositions all the batches had their [Ca + Cu]/P molar ratio below 1.500 (number of levels = 1).

Statistics: As detailed in the supplementary files, the statistical methods used in the manuscript include Analysis of Variance (ANOVA), post-hoc comparisons with Bonferroni correction, and Dunnett's test. A two-sided test was also used to determine the significance of a slope. ANOVA was the primary method for determining the statistical significance of various factors on different responses. Factors analyzed included: (A) The Cu content: The weight percentage of Cu in the samples. (B) The [Ca + Cu]/P molar ratio: low = "< 1.50", high = "> 1.50". (C) The Cell culture type: The conditions with no cells (NC), macrophages (MA), and osteoclasts (OC). (D) Repetition: The number of experimental runs (n = 3). Responses measured included lattice parameters, unit cell volume, SSA values, grain sizes, relative densities, TRAP activity, mean resorbed depth, and various ion concentrations (Ca, P, Cu, Na, K, Mg) in the cell medium. When the ANOVA results showed a significant difference, post-hoc comparisons with Bonferroni correction were used to pinpoint which specific group comparisons were statistically significant. The results of these comparisons are often presented with a p-value and an arrow indicating whether the response significantly increased (↗) or decreased (↘). The Dunnett's test was specifically used to compare the concentrations of Ca, P, and Cu ions from different cell culture types (no cells, macrophages, and osteoclasts) against a control group, which was the basal concentration in the cell culture medium alone.

3. Results

According to ICP-MS and XRD data (Figs. 1 and 2), the synthesis of Cu-free and Cu-doped β-TCP was successful, thereby confirming the visual impression given by the increasingly blue color of the samples up to 1.4 wt% and XPS surface analysis data (Figs. S1 and S2). ICP-MS analysis confirmed the presence of Cu in Cu-doped β-TCP (Fig. 1). Cu uptake exhibited a strong linear relationship with solution concentration (r^2 = 0.999), although the Cu relative content in the doped β-TCP was only 78% of that in solution, indicating that Cu incorporation into CDHA is slightly less favorable than Ca. The mean [Ca + Cu]/P molar ratio determined for all synthesized powders by ICP-MS was 1.498 ± 0.003, with values ranging from 1.490 to 1.512. In line with ICP-MS, Rietveld refinement revealed a linear increase in Cu content within the β-TCP phase with rising Cu concentration in the precipitation solution (Fig. 1), although the Cu content was markedly lower than the value measured by ICP-MS (50% vs 78%). Among the 43 elements analyzed by ICP-MS, only trace amounts of Sr (~22 ppm) were detected in the powders,

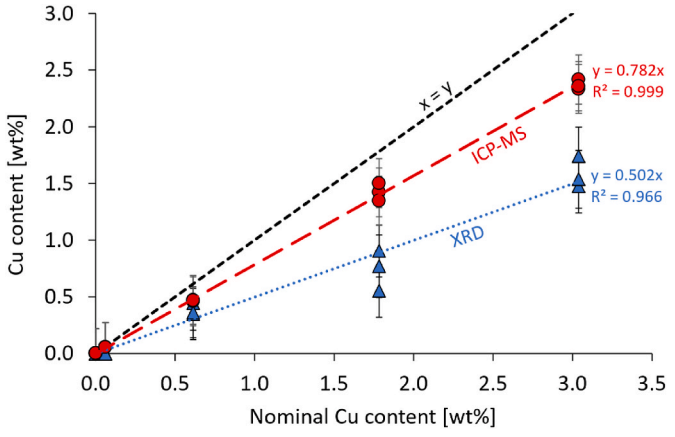

Fig. 1. Cu content of Cu-doped β-TCP as measured by ICP-MS (red) and XRD (blue). The Cu content is expressed as the copper weight divided by β-TCP weight. A nominal Cu content of 3.04 wt% corresponds to a molar content of 5.00 mol%. The difference between the Cu-content determined by XRD and ICP-MS suggests the formation of a Cu-rich secondary phase. (For interpretation of the references to color in this figure legend, the reader is referred to the Web version of this article.)

indicating a very low level of unintended elemental impurities, in particular of heavy metals. On this basis, the reference Cu-free β-TCP can be considered highly pure with respect to trace-element contamination.

XRD Rietveld refinement of CDHA powders heat-treated at 1000 °C for 15 h exposed β-TCP as the dominant phase, with occasional minor amounts of β-calcium pyrophosphate (β-CPP; $Ca_2P_2O_7$) detected (Fig. 2a). At the highest Cu loading, a diffraction peak corresponding to CuO appeared (Fig. 2b), suggesting the presence of trace CuO. A shift in the main β-TCP diffraction peak (Fig. 2c) further indicated partial incorporation of Cu into the β-TCP crystal lattice. Cu doping led to a significant decrease ($p < 0.001$) in both lattice parameters "a" and "c" (Fig. 3; Table S1), resulting in a notable reduction in unit cell volume (Fig. 3c). There was no significant interaction between Cu doping and [Ca + Cu]/P molar ratio (Fig. S3). The refinement also indicated that Cu substitution occurred preferentially at the Ca(5) crystallographic position (Fig. 3d).

Cu doping did not significantly alter the morphology of the CDHA powders (Fig. 4a–c,e,g), which consisted of agglomerated, globular particles with diameters below 100 nm. However, Cu doping notably increased the specific surface area (SSA) of the powders, from approximately 100 m^2/g to 160 m^2/g (Fig. 5a; Fig. S4a; Table S2, Table S3), indicating still an influence on the synthesis process. Following thermal treatment at 850 °C, Cu had no discernible effect on the SSA, which decreased to around 6 m^2/g (Fig. 5b). An increase of the [Ca + Cu]/P molar ratio significantly increased the SSA value ($p < 0.0001$) (Fig. S4b). Morphologically, the thermally treated powders exhibited a typical sintered structure, characterized by agglomerated rounded particles (Fig. 4b–d,f,h).

Microstructurally, the presence of Cu significantly affected the grain size and relative density of sintered samples ($p < 0.01$; Fig. 5; Fig. 6; Fig. S5; Table S4). Cu doping increased the grain size and density, with a local maximum at 0.1-0.5% Cu (Table S5). Small radiodense particles and particle agglomerates were found at grain boundaries in the samples with 1.4 and 2.4 wt% Cu loading (Fig. 6d,e,f). An EDX analysis at 2.4% Cu loading demonstrated the presence of Cu oxide (Fig. 6g and h), in line with the XRD results (Fig. 2b).

TRAP staining confirmed osteoclast presence (identified as TRAP-positive multinucleated cells) on both undoped and Cu-doped β-TCP cylinder surfaces (Fig. 7). Qualitative observations suggested a lower number of osteoclasts on β-TCP cylinders containing 0.5, 1.4, and 2.4 wt % Cu compared to the undoped and 0.1 wt% Cu-doped samples. Additional TRAP stained images (Fig. S6) further illustrate osteoclast development prior to and after 24 h of osteoclastic resorption. Quantitative analysis of TRAP activity revealed no statistically significant influence of Cu concentration (Fig. 7f) or the [Ca + Cu]/P molar ratio (Fig. S7a) on enzymatic activity (Table S6). However, TRAP activity levels in control media lacking osteoclasts (i.e., without cells or containing only macrophages) were significantly lower ($p < 0.001$; Fig. S7b; Table S7). Qualitatively, the proliferation of osteoclast progenitors (OCPs) seemed unaffected or only slightly affected by Cu-doping, whereas OCP fusion and activity were decreased.

The SEM micrographs illustrating the surfaces of both undoped and Cu-doped β-TCP cylinders, before and after exposure to cell culture conditions, are presented in Fig. 8. Before undergoing resorption, the surfaces of the cylinders appeared similar, except for the samples containing 2.4 wt% Cu, which exhibited increased porosity. When immersed in culture media without cells, the cylinders showed slight surface dissolution, which became more pronounced with the addition of HCl (Fig. 8). This degradation predominantly followed the polishing marks and grain boundaries. Comparable surface dissolution was observed in samples exposed to macrophages, regardless of Cu content. In contrast, cylinders cultured with osteoclasts showed grain resorption accompanied by the appearance of aligned needle-like structures on their surfaces. This was most evident in both pure β-TCP and the 0.1 wt% Cu-doped variants (Fig. 8; Fig. S8). Samples with 0.5 wt% and 1.4 wt% Cu doping displayed reduced signs of resorption, while those with 2.4 wt

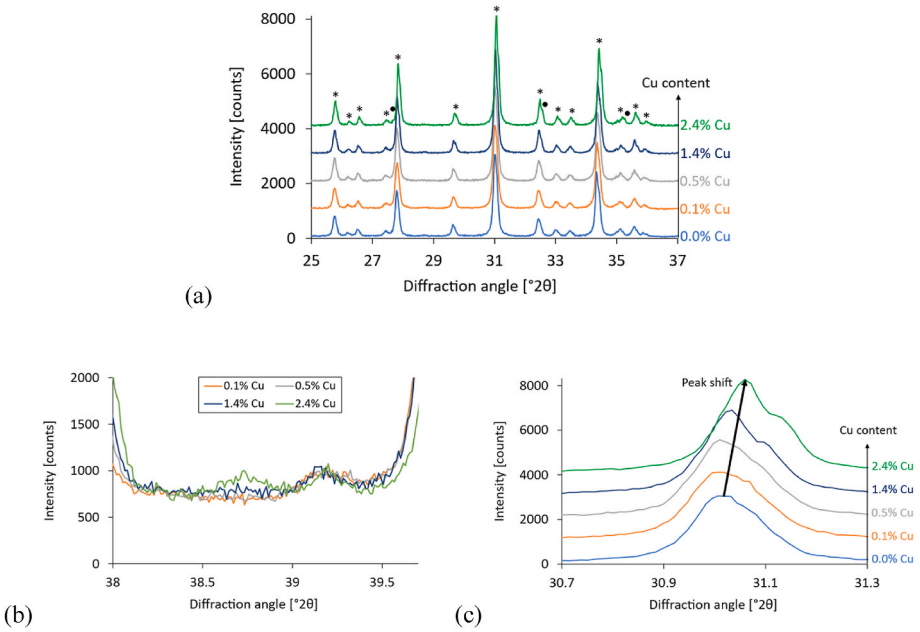

Fig. 2. (a) XRD diffraction patterns of Cu-doped β-TCP powders with identification of β-TCP (* symbols) and (● symbols) β-CPP peaks between 25 and 37 °2θ (a); (b) Appearance of the strongest CuO diffraction peak (PDF No 04-007-1375; 111 peak) on XRD spectra of Cu-doped β-TCP powders with increasing Cu content; (c) peak shift due to the increase in Cu content. The β-CPP peaks observed in the 2.4 wt% Cu-doped β-TCP are not representative, since no significant increase in β-CPP content is observed with increasing Cu content.

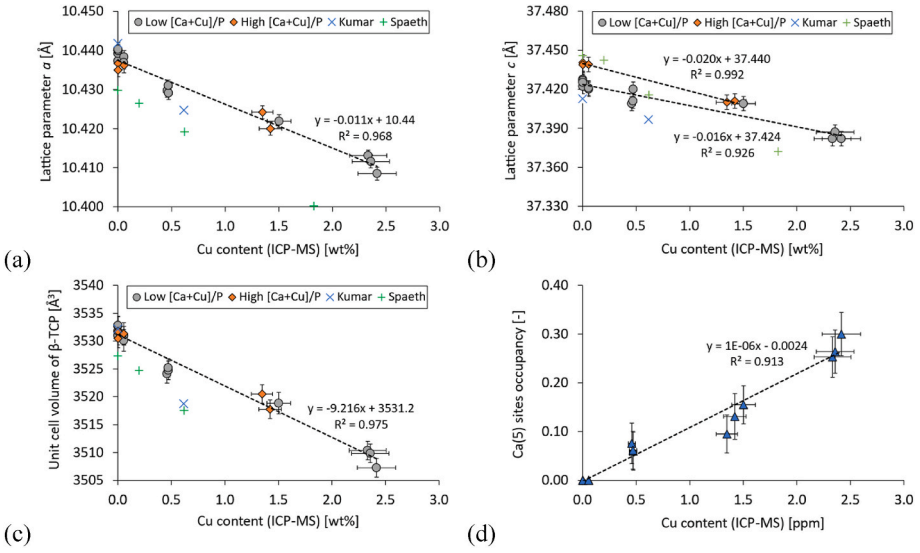

Fig. 3. Evolution of β-TCP (a) lattice parameter "*a*", (b) lattice parameter "*c*", (c) unit cell volume and (d) Ca(5) site occupancy with the Cu content. The [Ca + Cu]/P molar ratio is represented by (●) when below 1.500 and by (◆) when above 1.500. Changes in the lattice parameters, unit cell volume and Ca(5) site occupancy were highlighted with linear regressions (black dashed lines). Experimental data was compared with results from Kumar et al. [43] (blue × symbols) and Spaeth et al. [42] (green + symbols). Error bars for Cu content represent the uncertainty $U_{k=2}$, while error bars for the lattice parameters, unit cell volume and Ca sites occupancy stand for the repeatability (2.77*estimated standard deviation ESD). (For interpretation of the references to color in this figure legend, the reader is referred to the Web version of this article.)

% Cu exhibited only minor dissolution along grain boundaries and polishing lines.

Fig. 9 illustrates the post-resorption surface topography of pure and Cu-doped β-TCP cylinders, highlighting the relationship between surface features and Cu concentration. In these images, green denotes the reference plane, while blueish tones indicate recessed areas. For reference, the surface profiles of samples incubated in cell culture medium without cells are also provided (Fig. 9). Evidence of osteoclastic resorption was observed in cylinders with up to 0.5 wt% Cu, with no clear resorption marks in those with higher Cu levels, the blueish coloration in those cases corresponded to inherent porosity and/or pores possibly created by the loss of CuO agglomerates. Notably, the 0.1 wt% Cu-doped cylinders exhibited a morphological shift in the resorption pattern with deeper and more localized resorption pits (Fig. 9d).

Osteoclastic resorption of the Cu-doped β-TCP samples was significantly affected by the Cu content ($p < 0.001$; Fig. 10a, Table S8). Whereas no significant difference could be detected between 0 and 0.1 wt% doping (Table S9), further addition of Cu led to a significant drop of resorption. There was in fact no statistically significant difference of resorption between the groups "no cells", "macrophages", and

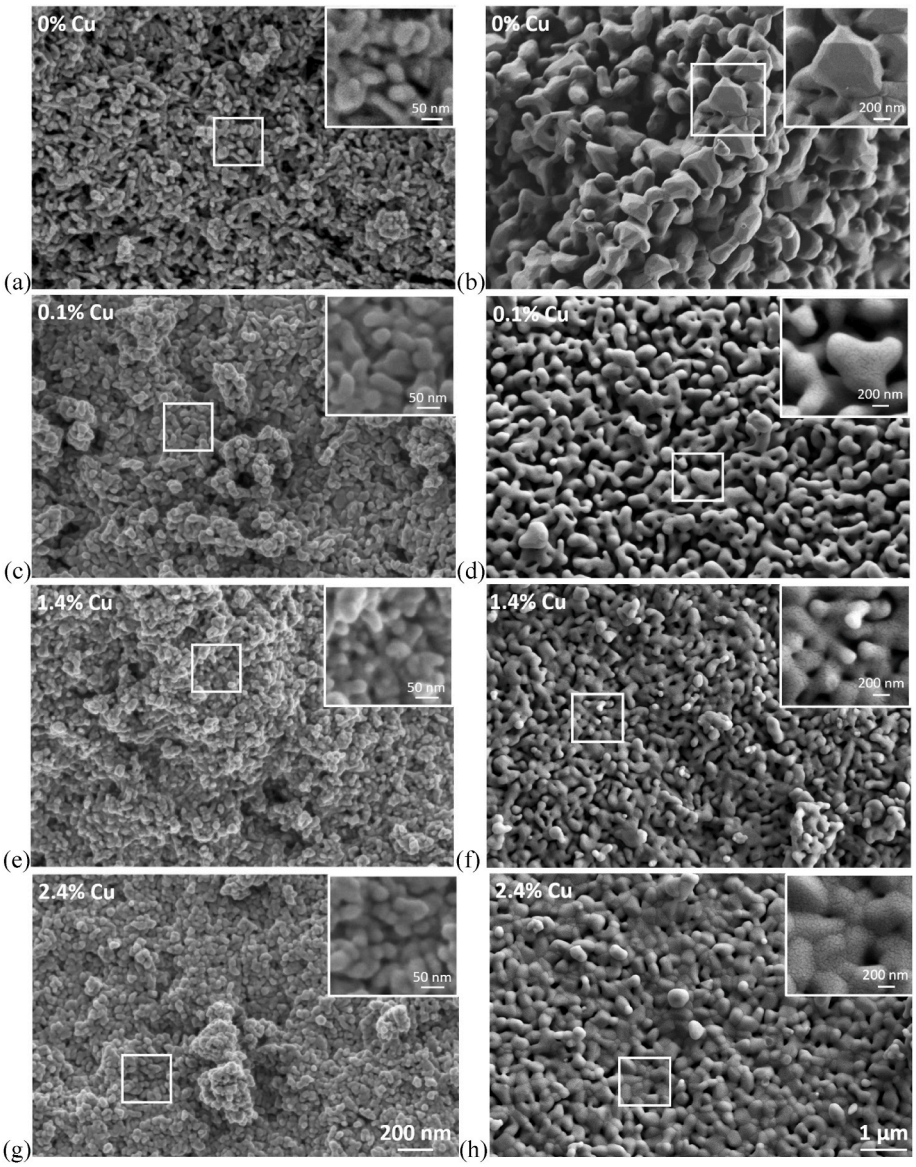

Fig. 4. Representative SEM images of undoped and Cu-doped CDHA (left column) and β-TCP (right column). The ICP-MS Cu content is indicated on the images (0%, 0.1%, 1.4%, 2.4%). The images in (a) and (b) are taken from Ref. [46]. The scale bar in (g) applies to (a), (c), and (e) while the one in (h) applies to (b), (d) and (f).

"osteoclasts" at 0.5 wt%, 1.5 wt%, and 2.4 wt% Cu doping (Fig. S9; Table S10), suggesting that osteoclastic resorption was fully inhibited at these Cu contents. A strong positive correlation was found between resorbed masses calculated via WLI and those derived from ICP-MS measurements (Fig. 10b; $R^2 = 0.75$; $p < 0.001$), confirming consistency between the two methods.

Fig. 11 presents the concentrations of Ca, P, and Cu ions in the culture medium following 24 h of cell culture experiments. The levels of Ca and phosphate ions were significantly influenced by both the type of cell culture ($p < 0.001$) and the Cu content in the β-TCP cylinders ($p < 0.01$) (Fig. 11; Table S11). Ca and P concentrations were notably higher in media containing osteoclasts compared to those with macrophages or no cells (Fig. 11a and b; Table S12). Further analysis revealed that for pure and 0.1 wt% Cu-doped β-TCP cylinders, Ca and phosphate levels were significantly elevated relative to baseline ($p < 0.001$; Table S13). For the 0.5 wt% Cu-doped samples, both the Ca and phosphate concentration also significantly exceeded baseline values (Fig. 11b; $p < 0.04$ and $p < 0.01$, respectively).

Cu ion concentration was strongly correlated with the Cu content in the β-TCP cylinders ($p < 0.001$; Fig. 11c; Table S11). Cu levels in Cu-free samples were not significantly different from the limit of detection (LOD; 0.4 µM), indicating that the samples were either truly Cu-free or contained Cu at concentrations close to the detection limit. The Cu ion concentration was significantly higher in the medium exposed to 2.4 wt % Cu-doped cylinders compared to the baseline ($p < 0.001$; Table S13). Elevated Cu levels were also observed in the 0.5 and 1.4 wt% Cu-doped samples ($p < 0.01$; Table S13). Sodium, potassium, and magnesium ion concentrations remained stable across all experimental conditions, showing no dependence on cell culture type, Cu content, or [Ca + Cu]/P molar ratio (Fig. S10, Table S11).

4. Discussion

This study sought to clarify how Cu incorporation, and any subsequent grain-boundary segregation, modifies β-TCP surface chemistry and microstructure, and how those alterations impact osteoclastic resorption. To this end, Cu-doped β-TCP was synthesized via a two-step process: first, Cu-substituted CDHA with a [Ca + Cu]/P molar ratio of 1.50 was precipitated; then, these precursor powders underwent a high-temperature phase transformation to yield Cu-doped β-TCP.

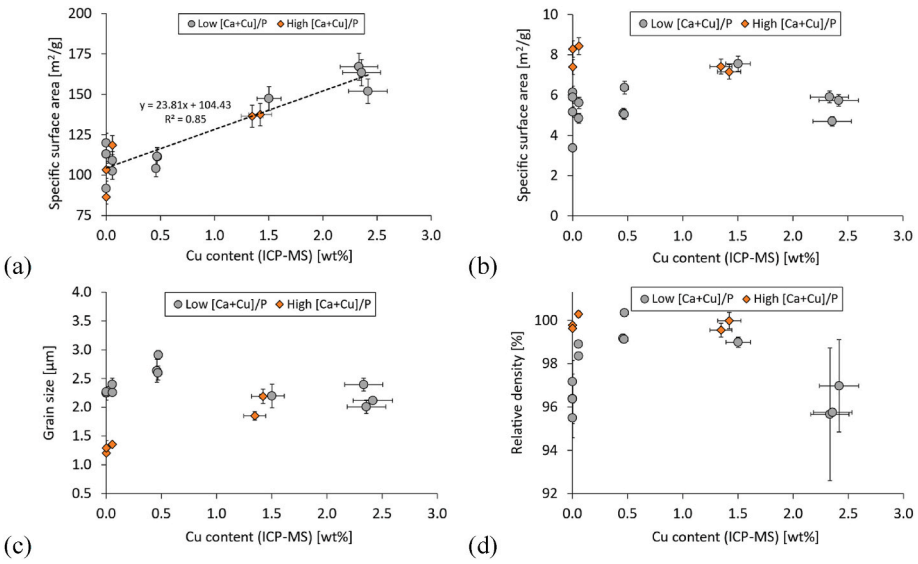

Fig. 5. Specific surface area (SSA) as a function of the Cu content (a) for CDHA powders and (b) for thermally treated β-TCP powders (1 h at 850 °C). (c) Grain sizes and (d) relative densities of pure and Cu-doped β-TCP cylinders after sintering as a function of the Cu content. The results are represented by (● symbols) when the [Ca + Cu]/P molar ratio is below 1.500 and by (◆ symbols) when above 1.500. Error bars for the SSA and the Cu content (ICP-MS) represent the uncertainty $U_{k=2}$. Error bars for the grain size ($n = 3$; 900 grains) and the relative density ($n = 3$) stand for the standard deviation. Note that the SSA values for pure CDHA and β-TCP powders, grain sizes and relative densities for pure β-TCP cylinders were published by Le Gars Santoni et al. [11].

The partial substitution of Ca nitrate with Cu nitrate in the solution did not significantly alter the precipitation reaction or the appearance of the reaction product (Fig. 4). However, the presence of Cu led to an increase in the specific surface area (SSA) of the powder, from approximately 100 m^2/g without Cu to 160 m^2/g at the highest Cu doping level ($p < 0.001$; Fig. 5). This trend suggests that Cu either promotes apatite nucleation, inhibits crystal growth, or affects both processes, consistent with findings from previous studies [53,54]. In contrast, another study focused on phosphate removal from wastewater also reported growth inhibition by Cu but observed an increase in crystal size [55]. The observed suppression of crystal growth could be attributed to the strong sorption of Cu ions onto apatite surfaces [56–58]. During heating at 850 °C, CDHA undergoes phase transformation and significant atomic diffusion, which promotes particle coalescence and grain growth, thereby erasing surface-adsorption effects present at low temperature. At this stage, Cu is either incorporated into the β-TCP crystal lattice or redistributed, so that it no longer effectively limits grain growth, explaining why the SSA of β-TCP powders is not affected by the Cu content.

The production of Cu-doped β-TCP by thermal treatment of Cu-doped CDHA powders was successful. Increasing the nominal Cu content during synthesis led to a corresponding increase in the Cu concentration in the resulting CDHA/β-TCP powders (Fig. 1). Minor deviations from the target [Ca + Cu]/P molar ratio of 1.500 were observed, along with trace amounts of secondary phases (HA and β-CPP), whose combined content remained below 1.1 wt%. These deviations are primarily attributed to batch-to-batch variations and incomplete incorporation of Cu into the crystal structure, as discussed above and below. The average Cu incorporation efficiency, determined by ICP-MS data was approximately 78% (Fig. 1).

The water content of the Cu nitrate used in the synthesis was unknown and assumed to be zero, therefore, incorporation efficiencies below 100% may partly result from an overestimation of the Cu content in the precursor salt. Such an overestimation would also be expected to affect the [Ca + Cu]/P molar ratio, specifically a decrease with increasing nominal Cu content, which was not observed. Also, the limited incorporation of Cu in apatite has already been reported [53,59]. Since deviations of the Ca/P molar ratio around 1.50 modifies grain size, density, crystallographic structure, and osteoclast response [11,46,60], a difference was made in the presentation of the results for powders with a [Ca + Cu]/P molar ratio below and above 1.50 ("low" and "high", respectively). The results suggest that the main influencing factor is the Cu content rather than the [Ca + Cu]/P molar ratio. This is in particular true for the osteoclastic response (Fig. S11).

XRD analysis confirmed that Cu was successfully integrated into the β-TCP crystal lattice (Figs. 2 and 3; Table S1). The lattice parameters "*a*" and "*c*", as well as the unit cell volume, decreased linearly with increasing Cu content (Fig. 3), consistent with Vegard's law [61]. This lattice contraction aligns with previous findings [42,43] and is attributed to the smaller ionic radius of Cu^{2+} compared to Ca^{2+}. Similar substitution behavior has been observed for other divalent cations with ionic radii smaller than that of Ca^{2+}, including Mg^{2+} [62] and Zn^{2+} [63]. Structural analyses and theoretical modeling further indicate a preferential substitution of Cu^{2+} at the Ca(5) crystallographic site within the β-TCP crystal lattice (Fig. 3d) [42,43,64]. However, the discrepancy between the Cu content measured by XRD, known to provide reliable estimates of lattice-incorporated dopants [42], and the higher values measured by ICP-MS (Fig. 1) suggests that not all Cu was retained within the β-TCP crystal lattice. Consistent with these findings, SEM, XRD, and EDX analyses (Figs. 2 and 6b) revealed CuO precipitates localized at β-TCP grain boundaries. Bazin et al. [65] demonstrated that CuO secondary phases observed in Cu-substituted CaP can be suppressed or eliminated by rapid cooling, whereas slow cooling promotes CuO formation at grain boundaries. Similar conclusions were drawn from in-situ high-temperature diffraction studies by Bulina et al. [66], who showed that Cu can temporarily reincorporate into the CaP lattice at elevated temperatures but segregates as CuO upon slow cooling. These results suggest that CuO seggregation occurred during the cooling step following Cu-doped β-TCP sintering.

In addition to altering the color of the material, first in blue and then in dark grey (Fig. S1), Cu doping markedly affected several physical properties of the material (Fig. 5; Table S4, Table S5). β-TCP grain size initially increased with increasing Cu content, reaching a maximum at 0.5 wt%, but decreased significantly at higher Cu concentrations (1.4 and 2.4 wt%) (Fig. 5c; Table S5). The origin of the maximum grain size observed at 0.5 wt% doping remains unclear. In contrast, the influence of Cu doping on density was less systematic. This variability may be partly attributed to the small deviations in the [Ca + Cu]/P molar ratio,

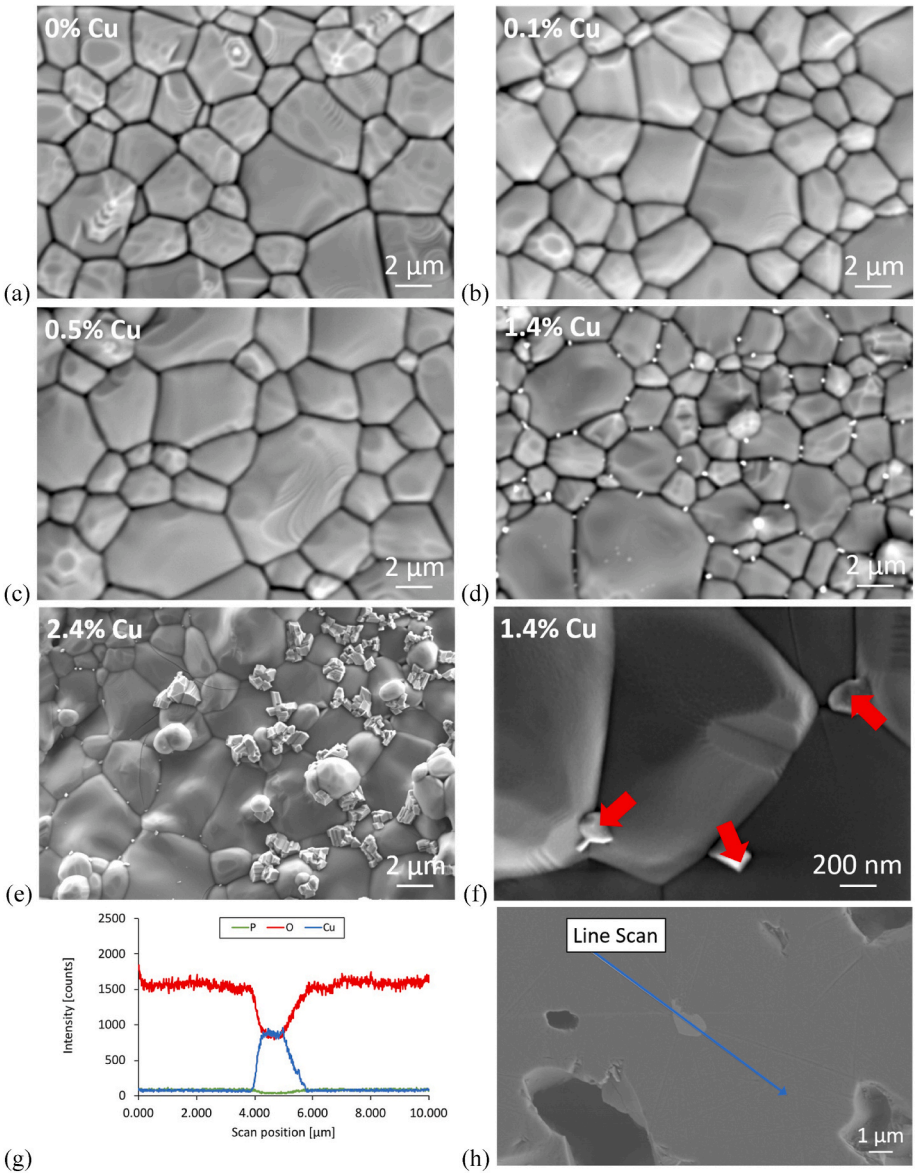

Fig. 6. Representative SEM-BSE images showing the evolution of the microstructure of dense β-TCP samples as a function of the Cu content. (a) 0%; (b) 0.1%; (c) 0.5%; (d) 1.4 wt% and (e) 2.4 wt% Cu-doped β-TCP cylinders. (f) Enlargement of the microstructure of 1.4 wt% Cu-doped β-TCP showing some of the crystals at the grain boundaries (red arrows). In addition, an SEM-EDX line scan (g) was performed on one of the Cu-rich precipitate in a 2.4 wt% Cu-doped β-TCP cylinders (h), showing an increase in Cu content and a decrease in O content as well as a slight decrease in P content. (For interpretation of the references to color in this figure legend, the reader is referred to the Web version of this article.)

which likely obscure the intrinsic effect of Cu on densification (Table S4). While most Cu-doped cylinders exhibited slightly higher densities, the 2.4 wt% Cu-doped samples showed a marked decrease (Fig. 5). This reduction in density could be due to the presence of abundant CuO precipitates at grain boundaries (Fig. 6), which hindered proper densification during sintering (Fig. 5; Table S5). Comparable effects of Cu on grain size and relative density were also reported by Nikita et al. in Cu-doped HA ceramics [67]. While they suggested that Cu segregation at HA grain boundaries might explain these changes, this mechanism was not explicitly demonstrated in their study.

TRAP staining confirmed the presence of osteoclasts on the surfaces of both pure and Cu-doped β-TCP cylinders (Fig. 7). Despite clear differences in resorptive activity, quantification of TRAP activity showed no significant differences between pure and Cu-doped samples (Fig. 7f; Table S6, Table S7). This lack of correlation between TRAP activity and osteoclastic resorption is consistent with previous reports [11,33] and indicates that Cu does not inhibit osteoclast formation or survival, but rather affects their functional activity.

After 24 h in cell culture medium, the surfaces of the β-TCP cylinders showed slight signs of dissolution, occurring predominantly along the grain boundaries and polishing lines (Fig. 8), consistent with past observations [11,60]. Although the cell culture solution was supersaturated with respect to β-TCP, it can be speculated that the mechanically induced surface defects associated with polishing lines possessed elevated surface energies and enhanced dissolution kinetics. Following osteoclastic resorption, only the pure and 0.1 wt% Cu-doped β-TCP cylinders exhibited clear evidence of resorption, characterized by the formation of highly oriented needle-like structures on the surface of resorbed grains and selective dissolution of grain boundaries (Fig. 8, Fig. S8). These needle-like structures are typically aligned along the c-axis of the β-TCP crystallographic lattice [49].

In contrast, cylinders with higher Cu contents (≥0.5 wt%) showed progressively reduced surface dissolution and ultimately no identifiable signs of osteoclastic resorption. These findings were corroborated by

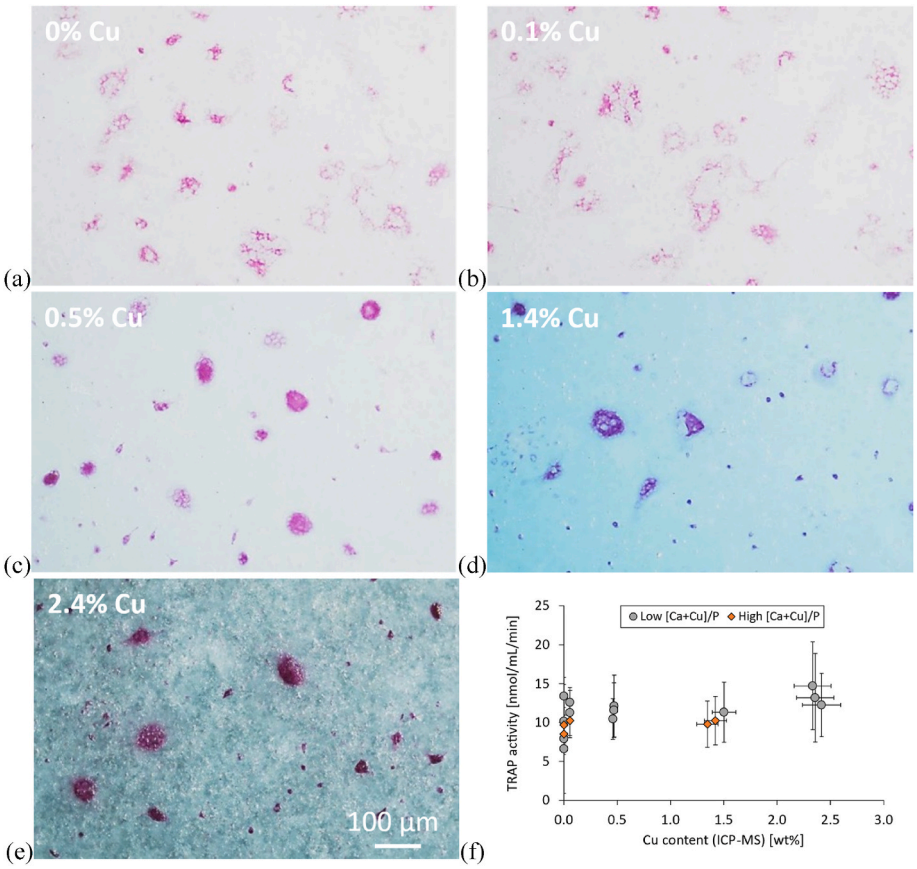

Fig. 7. Optical microscope images of TRAP stained osteoclasts on polished, pure and Cu-doped β-TCP cylinders at a doping level of (a) 0, (b) 0.1, (c) 0.5, (d) 1.4, and (e) 2.4 wt%; scale bar is 100 μm for all images. (f) Quantification of TRAP activity on pure and Cu-doped β-TCP cylinders after 24 h of cell culture experiment with osteoclasts (OC) as a function of the Cu content. The blue background observed in the stained images is due to the intrinsic color change caused by Cu doping (Fig. S1). Data were normalized by the mean of TRAP activity values in pure β-TCP cylinders for each cell culture experiment ($n = 3$). Error bars for the TRAP activity represent the standard deviations ($n = 3$) while they stand for the uncertainty $U_{k=2}$ for the Cu content. Note that among the $n = 3$ results from the control group, $n = 2$ had already been included in the $n = 5$ results previously published by Le Gars Santoni et al. 11 (For interpretation of the references to color in this figure legend, the reader is referred to the Web version of this article.)

WLI imaging (Fig. 9) and quantitative WLI analysis (Fig. 10), which demonstrated a significant reduction in resorption for the 0.5 wt% Cu-doped samples and an almost complete absence of resorption in the 1.4 and 2.4 wt% Cu-doped cylinders (Tables S8–S10). In fact, there was no significant difference in mean resorbed depth between the groups "no cells", "macrophages", and "osteoclasts" at 0.5 wt%, 1.5 wt%, and 2.4 wt % Cu doping (Fig. S9; Table S10). This Cu-dependent suppression of osteoclastic resorption is consistent with previous reports [41,44,68].

The analysis of Ca and phosphorus (P) ion concentrations in the cell culture medium corroborated the findings from SEM and WLI measurements (Figs. 8–11). Both pure and 0.1 wt% Cu-doped β-TCP cylinders released Ca and P at levels higher than baseline, consistent with active osteoclastic resorption of the CaP ceramic (Fig. 11, Table S11, Table S12). Notably, the 0.1 wt% Cu-doped samples released higher amounts of Ca and P than the undoped controls (Table S13), in agreement with WLI measurements; however, these differences did not reach statistical significance (Fig. 10a). The WLI pseudo-color images (Fig. 9) nevertheless revealed a qualitative shift in resorption morphology, showing fewer but distinctly deeper pits in the presence of 0.1 wt% Cu.

One possible explanation for this unexpected enhancement of localized resorption is a hypoxia-mimicking effect associated with low concentrations of released Cu^{2+}. Indeed, hypoxia has been shown to simultaneously increase osteoclastic resorption and decrease the resorbed area [69]. Cu ions has been reported to stabilize HIF-1α and activate HIF-1–dependent gene expression under normoxic conditions, thereby functioning as hypoxia mimetics in several cell types [70,71]. Such Cu-induced HIF-1α activation has also been described in Cu-releasing biomaterials, where it promotes pro-angiogenic and stromal responses [72], and parallels the hypoxia-mimicking behavior previously demonstrated for Co-doped CaP [41]. Thus, even trace Cu release from the 0.1 wt% Cu-doped β-TCP may have contributed to a microenvironment permissive to deeper, more localized osteoclastic resorption despite the overall similar extent of material degradation.

Even in the absence of cells, the Cu release into the cell culture medium as measured by ICP-MS increased sharply with the CuO content of the β-TCP cylinders (Fig. 11c). ICP-MS detected baseline Cu concentrations in the medium from either undoped cylinders or those doped with 0.1 wt% Cu (i.e. close to the limit of detection (LOD) of 0.4 μM). In contrast, Cu concentrations rose by approximately two orders of magnitude from ~2 μM at 0.5 wt% Cu to ~0.15 mM at 2.4 wt% Cu (Fig. 11c).

These concentrations substantially exceed the reported equilibrium solubility of CuO under physiological conditions by two to three orders of magnitude [73], indicating that the measured Cu levels cannot be explained by simple dissolution equilibria alone.

The collected supernatants were centrifuged prior to ICP-MS analysis (16,100×*g*, 10 min). Under these conditions, isolated CuO particles in the size range observed by SEM (Fig. 6f) would be expected to sediment efficiently. Nevertheless, ICP-MS inherently quantifies total Cu following acid digestion and does not allow discrimination between free Cu^{2+} ions, Cu complexed with constituents of the culture medium, or Cu originating from labile or nanoscale solid phases that may not sediment

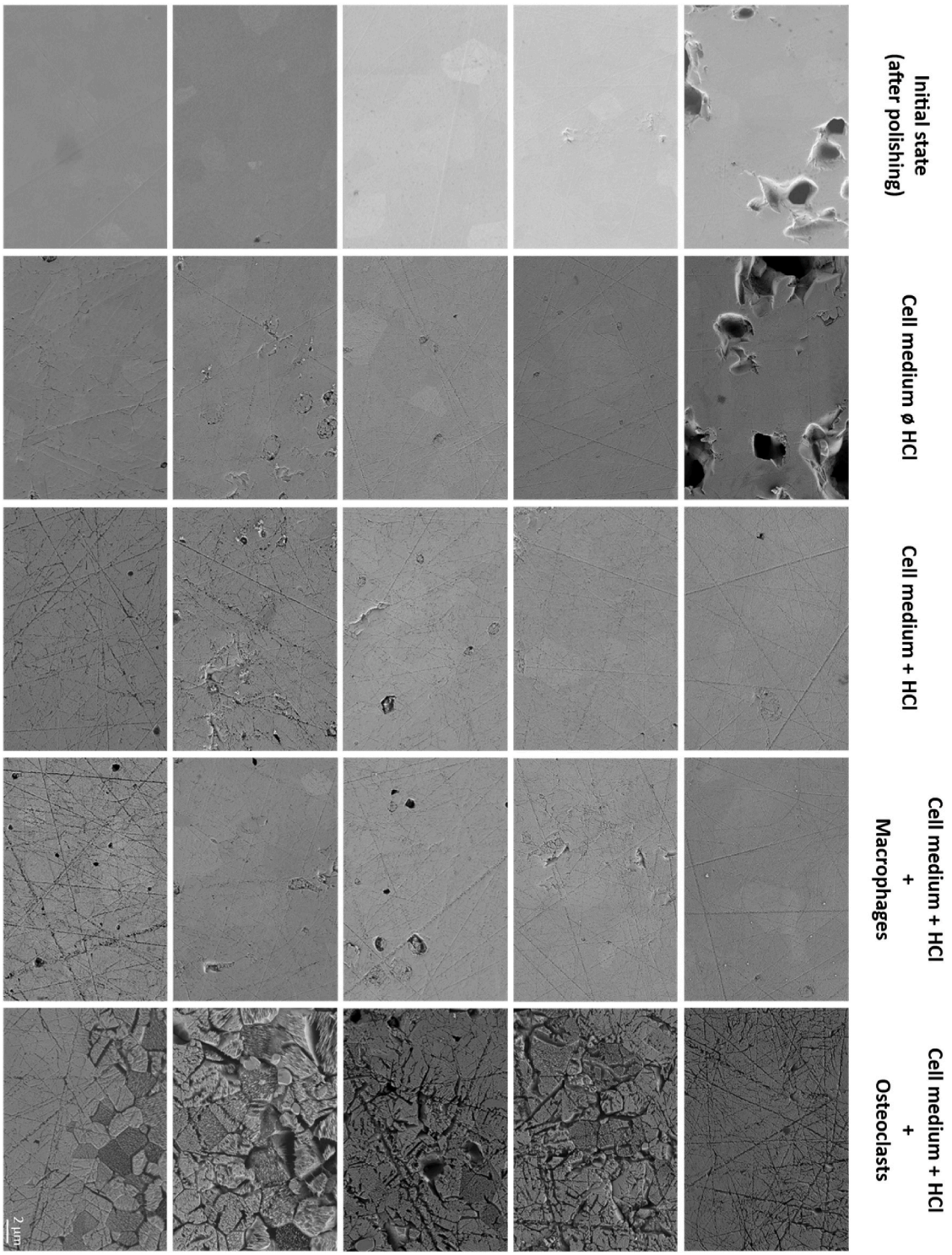

Fig. 8. Representative SEM images of the surface of selected pure and Cu-doped β-TCP cylinders (polished), before cell culture experiments, after 24 h in cell culture medium with and without HCl, with macrophages and with osteoclasts. The rows show the Cu-doping levels from 0 wt% (bottom row) to 2.4 wt% (top row). The columns (from left to right) show the sample surfaces (1st) after initial polishing, (2nd) after contacting the cell medium, (3rd) after contacting the cell medium and adding the diluted HCl solution, (4th) after contacting the cell medium, adding the diluted HCl solution, and cultivating macrophages during 24 h, and finally (5th) contacting the cell medium, adding the diluted HCl solution, and cultivating osteoclasts during 24 h. The 2 µm scale bar is valid for all the images. Note that SEM images for pure β-TCP cylinders were already published by Le Gars Santoni et al. [11].

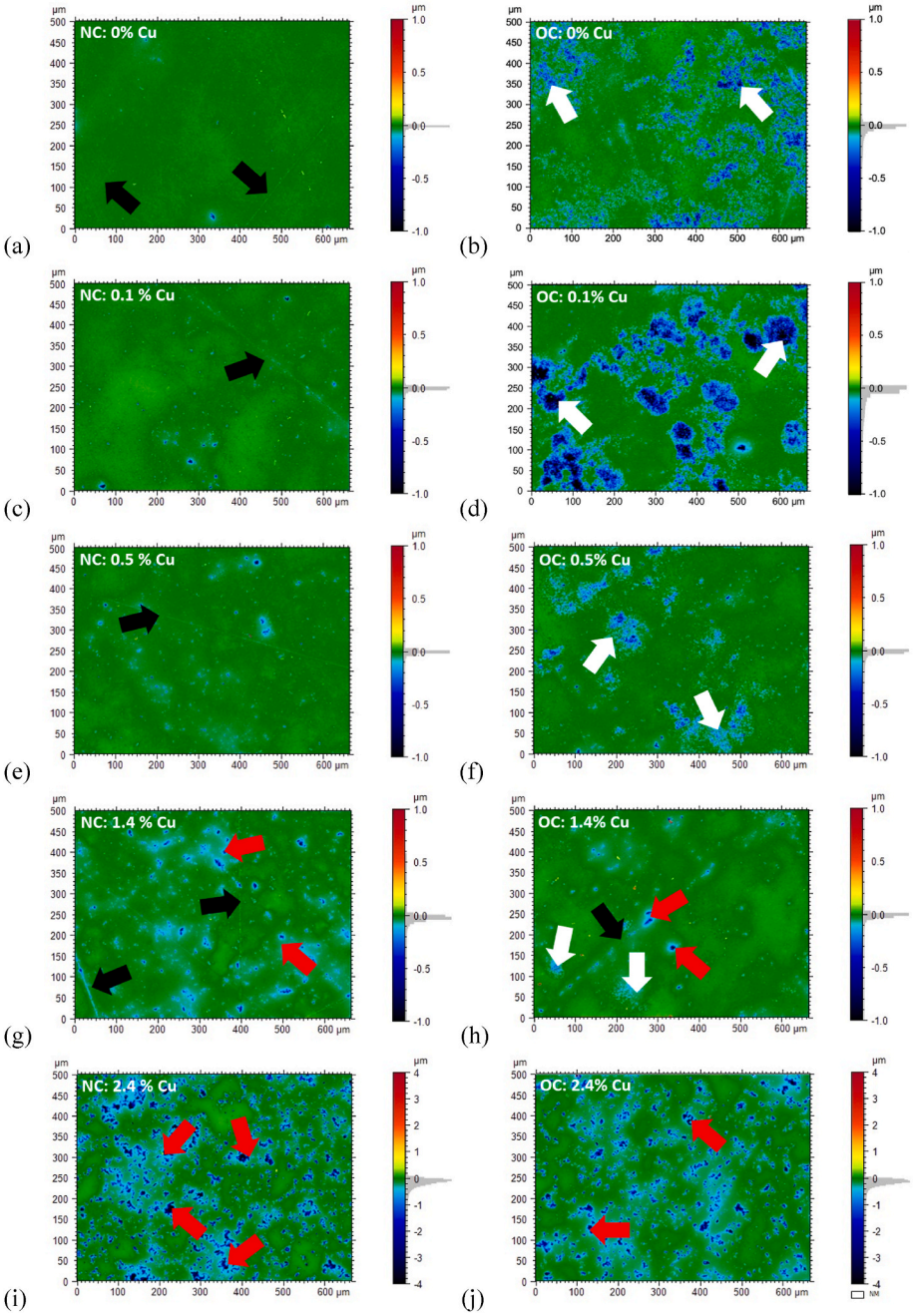

Fig. 9. Representative WLI pseudo-color images of the surface of pure and Cu-doped β-TCP cylinders (a, c, e, g, i) after 24 h in cell culture medium (with HCl) with no cells (NC) and (b, d, f, h, j) after 24 h of osteoclastic resorption: (a, b) 0 (c, d) 0.1, (e, f) 0.5, (g, h) 1.4, (i, j) 2.4 wt% Cu-doped β-TCP. White arrows show osteoclastic resorption zones; black arrows indicate some lines from mechanical polishing and red arrows some porosity in the 1.4 and 2.4 wt% Cu-doped β-TCP cylinders, possibly due to the release of CuO particles. Note that image (a) was already published by Le Gars Santoni et al. 11 (For interpretation of the references to color in this figure legend, the reader is referred to the Web version of this article.)

completely. Consequently, the measured Cu concentrations should be interpreted as total Cu present in the supernatant rather than as a direct measure of freely dissolved Cu^{2+}.

As a result, the actual bioavailable Cu^{2+} concentration in the cell culture medium remains difficult to determine. Under the given conditions, it is likely constrained by the solubility limits of Cu-containing phases. For CuO, reported equilibrium solubility values in aqueous media are on the order of 0.1–1.0 μM [73], and the solubility of Cu phosphate is similarly low. Accordingly, the ~2 μM Cu^{2+} detected in the medium from the 0.5 wt% Cu-doped cylinders likely overestimates the truly bioavailable dissolved Cu^{2+} fraction, with contributions from complexed Cu species or labile solid residues not resolvable by ICP-MS. Despite this uncertainty, previous studies have shown that even micromolar or sub-micromolar Cu^{2+} concentrations can significantly modulate osteoclast behavior. For example, Wilson et al. [44] showed that Cu sulfate concentrations of 1 μM and above significantly decreased *in vitro* osteoclastic resorption. while Zhang et al. reported inhibition of osteoclastic resorption at Cu^{2+} concentrations between 0.1 and 1 μM and stimulation at ~0.01 μM [74].

Importantly, irrespective of the precise Cu speciation in the medium, osteoclastic resorption was progressively suppressed and ultimately fully inhibited with increasing Cu doping of β-TCP. This indicates that the biological response correlates robustly with the presence of Cu-rich grain-boundary phases rather than requiring a precise quantification of

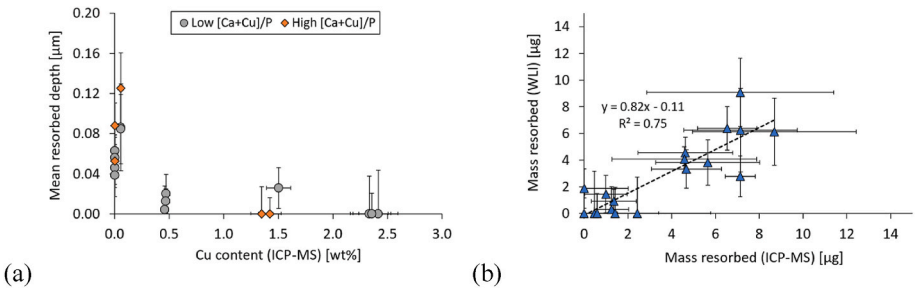

Fig. 10. (a) Mean resorbed depth of pure and Cu-doped β-TCP cylinders in contact with osteoclasts as a function of their bulk Cu content. (b) Correlation between masses resorbed by osteoclasts on the upper surface of pure and Cu-doped β-TCP cylinders, quantified by white light interferometry (y axis) and by ICP-MS (x axis) via phosphate release in the cell culture medium. The Pearson's correlation coefficient r was 0.87, R^2 value was 0.75 with $p < 0.001$. Mean resorbed depth values were normalized by those of pure β-TCP cylinders for each cell culture experiments ($n = 3$). Error bars for the mean resorbed depth represent the standard deviations ($n = 3$), while they stand for the $U_{k=2}$ values for Cu content. The error bars for the resorbed masses correspond to the standard deviations ($n = 3$). Note that the $n = 3$ raw data from the pure β-TCP cylinders were included in the $n = 6$ data already published by Le Gars Santoni et al. [11].

free extracellular Cu^{2+} concentrations. Additional fractionation approaches, such as ultrafiltration or ultracentrifugation prior to analysis, would be required to further resolve Cu speciation. Taken together, these observations indicate that the inhibition of osteoclastic resorption at higher Cu doping levels is most plausibly linked to the presence of Cu-rich grain-boundary phases, rather than to bulk β-TCP dissolution or to a narrowly defined extracellular Cu^{2+} concentration.

Such a dissociation between total Cu exposure and biological effect is consistent with previously reported biphasic Cu^{2+} responses in osteoclasts. Specifically, concentration-dependent redox effects have been proposed, whereby very low Cu^{2+} levels promote osteoclastogenesis via reactive oxygen species (ROS) signaling, while higher concentrations exert inhibitory or cytotoxic effects, potentially through oxidative stress–induced suppression or apoptosis [75]. This threshold-like behavior is consistent with the results of the present study and may explain the morphological shift in the resorption pattern observed in the lightly doped (0.1 wt%) β-TCP cylinders.

The central hypothesis of this study was that Cu segregation at the grain boundaries of Cu-doped β-TCP plays a key role in mediating its biological response. Our results partially support this hypothesis, as clear evidence of Cu segregation was observed in the form of CuO particles located at grain boundaries (Fig. 6). Moreover, increasing CuO content was associated with complete inhibition of osteoclast resorptive activity (Figs. 9 and 10). However, the observed inhibition may not be solely attributable to grain-boundary CuO, since Cu ions substituted within the β-TCP crystal lattice could also be released during osteoclastic attack and contribute to the biological response.

An important question concerns the biologically relevant concentration range. In the present study, this appears to correspond to Cu doping levels around 0.1 wt%, at which Cu incorporation modified osteoclast resorption pattern. This effect is more plausibly attributed to a direct modulation of osteoclast behavior than to an increase in β-TCP solubility induced by Cu substitution since the Cu-doped platelets incubated in SBF do not show increasing levels of dissolution (Fig. 8). Nevertheless, in vivo responses may differ substantially due to the greater complexity of living systems. Moreover, the rationale for deliberately increasing β-TCP resorption rates at the much higher levels typically reported in the literature [42,43,65,66,74,76,77] warrants careful consideration, as several studies have suggested that β-TCP may already resorb too rapidly under physiological conditions. Regarding the safety of Cu release during the resorption of Cu-doped β-TCP, both ISO 10993 biocompatibility standards and the United States Pharmacopeia (USP ⟨232⟩) specify a permitted daily exposure (PDE) for Cu of 300 µg/day for the parenteral route. At a Cu doping level of 0.1 wt%, identified in the present study as the optimal concentration, this PDE would correspond to the resorption of approximately 300 mg of β-TCP per day. This rate likely represents the upper bound of β-TCP resorption that would be expected to occur in vivo.

5. Conclusion

This work demonstrates that Cu doping strongly influences β-TCP microstructure, grain-boundary chemistry, and osteoclastic resorption *in vitro*. At higher doping levels (≥1.4 wt% Cu), excess Cu segregates to grain boundaries as CuO particles and is associated with a complete inhibition of osteoclast-mediated resorption. In contrast, at low doping levels (≤0.1 wt% Cu), Cu remains incorporated in the β-TCP lattice without CuO formation, and its release is triggered primarily by osteoclastic activity, resulting in a modest enhancement of resorption. While grain-boundary segregation of Cu as CuO was confirmed at higher doping levels, its specific contribution to the biological response could not be resolved. The results highlight a narrow compositional window near 0.1 wt% where Cu may influence osteoclastic resorption, while avoiding the inhibitory effects observed at higher concentrations. Given the complexity of in vivo environments and the ongoing debate over the desirability of increasing β-TCP resorption rates, further studies in animal models are warranted to assess the translational relevance of these *in vitro* results.

Declaration of generative AI and AI-assisted technologies in the manuscript preparation process

During manuscript preparation, the authors used ChatGPT (OpenAI) to assist with language refinement and clarity of author-written text and, on occasion, to identify potentially relevant literature. The AI tool was not used to generate scientific content, data, or interpretations. After using this tool/service, the authors reviewed and edited the content as needed and take full responsibility for the content of the published article.

CRediT authorship contribution statement

Bastien Le Gars Santoni: Conceptualization, Formal analysis, Investigation, Methodology, Visualization, Writing – original draft, Writing – review & editing. **Nicola Döbelin:** Conceptualization, Methodology, Software, Validation, Writing – review & editing. **Silvia Dolder:** Investigation. **Roman Heuberger:** Methodology, Software, Validation. **Yassine Maazouz:** Formal analysis, Writing – review & editing. **Christoph Stähli:** Methodology, Software, Validation, Writing – review & editing. **Paul Bowen:** Conceptualization, Funding acquisition, Project administration, Supervision, Writing – review & editing. **Willy Hofstetter:** Conceptualization, Resources, Supervision, Writing – review & editing. **Marc Bohner:** Conceptualization, Formal analysis, Funding acquisition, Investigation, Project administration, Resources, Supervision, Writing – review & editing.

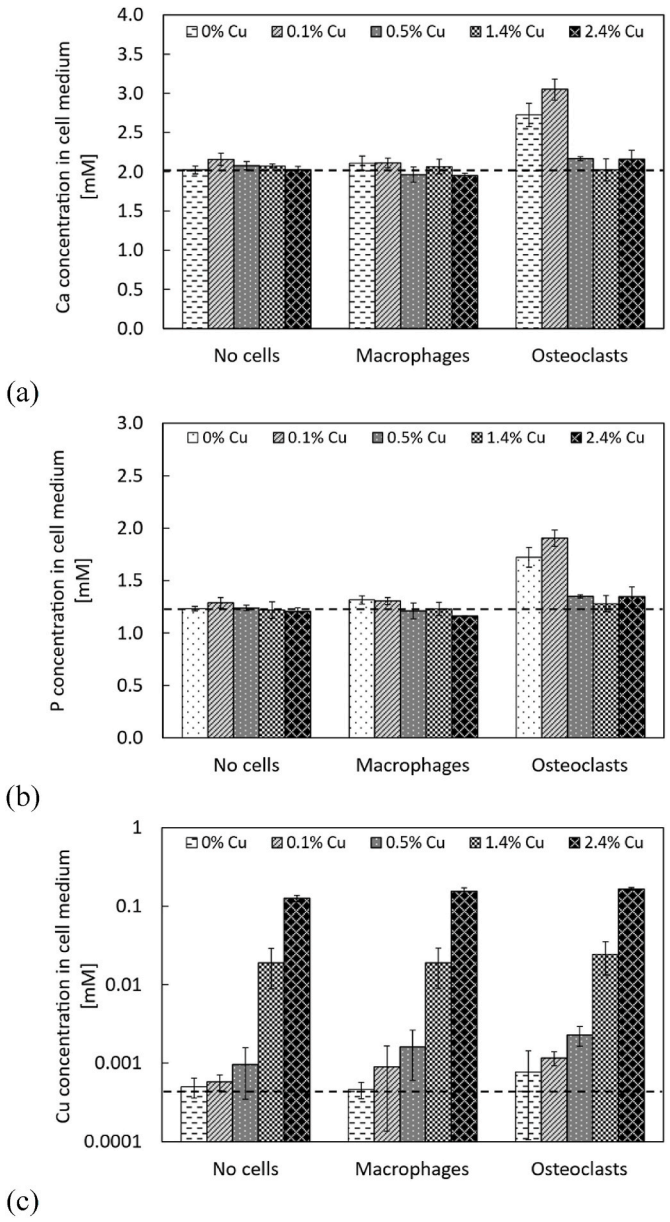

Fig. 11. ICP-MS ion concentrations of (a) Ca, (b) P, (c) Cu in cell culture medium after 24 h of contact between pure and Cu-doped β-TCP cylinders and cell culture medium with no cells (NC), macrophages (MA) and osteoclasts (OC). Note that for every composition, the mean of the three batches is displayed. The dashed horizontal lines represent the corresponding basal ion concentration in the cell culture medium: 2.04 ± 0.29 mM for Ca, 1.23 ± 0.13 mM for P, and <LOD for Cu. Data were normalized by the mean value of Na, K and Mg ion concentrations in each cell culture experiments (n = 3) to account for cell culture medium fluctuations. Error bars stand for standard deviations (n = 3). Cu levels in Cu-free samples were not significantly different from the limit of detection (LOD; 0.4 μM), indicating that the samples were either truly Cu-free or contained Cu at concentrations close to the detection limit. Note that the n = 3 raw data from the pure β-TCP cylinders were included in the n = 6 data already published by Le Gars Santoni et al. [11].

Declaration of competing interest

The authors declare that they have no known competing financial interests or personal relationships that could have appeared to influence the work reported in this paper.

Acknowledgements

The authors would like to thank Pascal Michel, Olivier Loeffel, Luzia Niggli, Gabrielle Sblendorio, Duncan Alexander and Isabelle Heimgartner for their support with the experiments, Jean-Christophe Hornez for his advice on the slip casting procedure and the Swiss National Science Foundation for its funding (Grant no. 200021_169027).

Appendix A. Supplementary data

Supplementary data to this article can be found online at https://doi.org/10.1016/j.mtbio.2026.103019.

Data availability

Data will be made available on request.

References

[1] P.V. Giannoudis, H. Dinopoulos, E. Tsiridis, Bone substitutes: an update, Injury 36 (Suppl 3) (2005) S20–S27, https://doi.org/10.1016/j.injury.2005.07.029.
[2] E.D. Arrington, W.J. Smith, H.G. Chambers, A.L. Bucknell, N.A. Davino, Complications of iliac crest bone graft harvesting, Clin. Orthop. Relat. Res. (1996) 300–309, https://doi.org/10.1097/00003086-199608000-00037.
[3] E.M. Younger, M.W. Chapman, Morbidity at bone graft donor sites, J. Orthop. Trauma 3 (1989) 192–195, https://doi.org/10.1097/00005131-198909000-00002.
[4] R. Dimitriou, G.I. Mataliotakis, A.G. Angoules, N.K. Kanakaris, P.V. Giannoudis, Complications following autologous bone graft harvesting from the iliac crest and using the RIA: a systematic review, Injury 42 (2011) S3–S15, https://doi.org/10.1016/j.injury.2011.06.015.
[5] R.Z. LeGeros, Properties of osteoconductive biomaterials: calcium phosphates, Clin. Orthop. Relat. Res. 395 (2002) 81–98, https://doi.org/10.1097/00003086-200202000-00009.
[6] M. Bohner, L. Galea, N. Doebelin, Calcium phosphate bone graft substitutes: failures and hopes, J. Eur. Ceram. Soc. 32 (2012) 2663–2671, https://doi.org/10.1016/j.jeurceramsoc.2012.02.028.
[7] P.S. Eggli, W. Müller, R.K. Schenk, Porous hydroxyapatite and tricalcium phosphate cylinders with two different pore size ranges implanted in the cancellous bone of rabbits. A comparative histomorphometric and histologic study of bony ingrowth and implant substitution, Clin. Orthop. Relat. Res. 232 (1988) 127–138, https://doi.org/10.1097/00003086-198807000-00017.
[8] I.R. Zerbo, A.L. Bronckers, G. de Lange, E.H. Burger, Localisation of osteogenic and osteoclastic cells in porous beta-tricalcium phosphate particles used for human maxillary sinus floor elevation, Biomaterials 26 (2005) 1445–1451, https://doi.org/10.1016/j.biomaterials.2004.05.003%20Get%20rights%20and%20content.
[9] S. Yamada, D. Heymann, J.M. Bouler, G. Daculsi, Osteoclastic resorption of calcium phosphate ceramics with different hydroxyapatite/b-tricalcium phosphate ratios, Biomaterials 18 (1997) 1037–1041, https://doi.org/10.1016/S0142-9612(97)00036-7.
[10] M. Jarcho, Calcium phosphate ceramics as hard tissue prosthetics, Clinical Orthopaedics and Related Research No. 157 (1981) 259–278, https://doi.org/10.1097/00003086-198106000-00037.
[11] B. Le Gars Santoni, L. Niggli, S. Dolder, O. Loeffel, G.A. Sblendorio, R. Heuberger, Y. Maazouz, C. Stähli, N. Döbelin, P. Bowen, W. Hofstetter, M. Bohner, Effect of minor amounts of β-calcium pyrophosphate and hydroxyapatite on the physico-chemical properties and osteoclastic resorption of β-tricalcium phosphate cylinders, Bioact. Mater. 10 (2022) 222–235, https://doi.org/10.1016/j.bioactmat.2021.09.003.
[12] S.J. Kalita, H.A. Bhatt, Nanocrystalline hydroxyapatite doped with magnesium and zinc: synthesis and characterization, Mater. Sci. Eng. C 27 (2007) 837–848, https://doi.org/10.1016/j.msec.2006.09.036.
[13] H.A. Bhatt, S.J. Kalita, Influence of oxide-based sintering additives on densification and mechanical behavior of tricalcium phosphate (TCP), J. Mater. Sci. Mater. Med. 18 (2007) 883–893, https://doi.org/10.1007/s10856-006-0091-0.
[14] G. Gasquères, P. Bonhomme, J. Maquet, F. Babonneau, S. Hayakawa, T. Kanaya, A. Osaka, Revisiting silicate substituted hydroxyapatite by solid-state NMR, Magn. Reson. Chem. 46 (2008) 342–346, https://doi.org/10.1002/mrc.2109.
[15] S. Torkornoo, M. Bohner, I. McCarroll, B. Gault, Optimization of parameters for atom probe tomography analysis of β-Tricalcium phosphates, Microsc. Microanal. 30 (2025) 1074–1082, https://doi.org/10.1093/mam/ozae077.
[16] P.R. Cantwell, M. Tang, S.J. Dillon, J. Luo, G.S. Rohrer, M.P. Harmer, Grain boundary complexions, Acta Mater. 62 (2014) 1–48, https://doi.org/10.1016/j.actamat.2013.07.037.
[17] G. Grass, C. Rensing, M. Solioz, Metallic copper as an antimicrobial surface, Appl. Environ. Microbiol. 77 (2011) 1541–1547, https://doi.org/10.1128/AEM.02766-10.
[18] D. Campoccia, L. Montanaro, C.R. Arciola, A review of the biomaterials technologies for infection-resistant surfaces, Biomaterials 34 (2013) 8533–8554, https://doi.org/10.1016/j.biomaterials.2013.07.089.

[19] L. Rio, E. Kusiak-Nejman, J. Kiwi, B. Bétrisey, C. Pulgarin, A. Trampuz, A. Bizzini, Comparison of methods for evaluation of the bactericidal activity of copper-sputtered surfaces against Methicillin-resistant Staphylococcus aureus, Appl. Environ. Microbiol. 78 (2012) 8176–8182, https://doi.org/10.1128/AEM.02266-12.

[20] H. Chai, L. Guo, X. Wang, Y. Fu, J. Guan, L. Tan, L. Ren, K. Yang, Antibacterial effect of 317L stainless steel contained copper in prevention of implant-related infection *in vitro* and *in vivo*, J. Mater. Sci. Mater. Med. 22 (2011) 2525–2535, https://doi.org/10.1007/s10856-011-4427-z.

[21] R. Uauy, M. Olivares, M. Gonzalez, Essentiality of copper in humans, Am. J. Clin. Nutr. 67 (1998) 952S–959S, https://doi.org/10.1093/ajcn/67.5.952S.

[22] G.R. Lee, S. Nacht, J.N. Lukens, G.E. Cartwright, Iron metabolism in copper-deficient swine, J. Clin. Investig. 47 (1968) 2058–2069, https://doi.org/10.1172/JCI105891.

[23] A. Dancis, D.S. Yuan, D. Haile, C. Askwith, D. Eide, C. Moehle, J. Kaplan, R. D. Klausner, Molecular characterization of a copper transport protein in S. cerevisiae: an unexpected role for copper in iron transport, Cell 76 (1994) 393–402, https://doi.org/10.1016/0092-8674(94)90345-X.

[24] I. Fridovich, Superoxide anion radical (O2.-), superoxide dismutases, and related matters, J. Biol. Chem. 272 (1997) 18515–18517, https://doi.org/10.1074/jbc.272.30.18515.

[25] S. Przedborski, E.A. Schon, Loss of ROS-a radical response, Nat. Genet. 18 (1998) 99–100, https://doi.org/10.1038/ng0298-99.

[26] P. Habibovic, J.E. Barralet, Bioinorganics and biomaterials: bone repair, Acta Biomater. 7 (2011) 3013–3026, https://doi.org/10.1016/j.actbio.2011.03.027.

[27] H.M. Kagan, W. Li, Lysyl oxidase: properties, specificity, and biological roles inside and outside of the cell, J. Cell. Biochem. 88 (2003) 660–672, https://doi.org/10.1002/jcb.10413.

[28] J. Barralet, U. Gbureck, P. Habibovic, E. Vorndran, C. Gerard, C.J. Doillon, Angiogenesis in calcium phosphate scaffolds by inorganic copper ion release, Tissue Eng Part A 15 (2009) 1601–1609, https://doi.org/10.1089/ten.tea.2007.0370.

[29] G. Hu, Copper stimulates proliferation of human endothelial cells under culture, J. Cell. Biochem. 69 (1998) 326–335, https://doi.org/10.1002/(SICI)1097-4644(19980601)69:3%3C326::AID-JCB10%3E3.0.CO;2-A.

[30] J.P. Rodríguez, S. Ríos, M. González, Modulation of the proliferation and differentiation of human mesenchymal stem cells by copper, J. Cell. Biochem. 85 (2002) 92–100, https://doi.org/10.1002/jcb.10111.

[31] B.J. Smith, J.B. King, E.A. Lucas, B.H. Arjmandi, B.J. Stoecker, M.P. Akhter, Skeletal unloading and dietary copper depletion are detrimental to bone quality of mature rats, J. Nutr. 132 (2002) 190–196, https://doi.org/10.1093/jn/132.2.190.

[32] L.M. Klevay, Cardiovascular disease from copper deficiency—A history, J. Nutr. 130 (2000) 489S–492S, https://doi.org/10.1093/jn/130.2.489S.

[33] A. Bernhardt, J. Bacova, U. Gbureck, M. Gelinsky, Influence of Cu2+ on osteoclast formation and activity *in vitro*, IJMS 22 (2021) 2451, https://doi.org/10.3390/ijms22052451.

[34] P. Ferenci, Diagnosis and current therapy of Wilson's disease, Aliment. Pharmacol. Ther. 19 (2004) 157–165, https://doi.org/10.1046/j.1365-2036.2003.01813.x.

[35] A. Hoppe, R. Meszaros, C. Stähli, S. Romeis, J. Schmidt, W. Peukert, B. Marelli, S. N. Nazhat, L. Wondraczek, J. Lao, E. Jallot, A.R. Boccaccini, *In vitro* reactivity of Cu doped 45S5 bioglass® derived scaffolds for bone tissue engineering, J. Mater. Chem. B 1 (2013) 5659, https://doi.org/10.1039/c3tb21007c.

[36] A. Hoppe, N.S. Güldal, A.R. Boccaccini, A review of the biological response to ionic dissolution products from bioactive glasses and glass-ceramics, Biomaterials 32 (2011) 2757–2774, https://doi.org/10.1016/j.biomaterials.2011.01.004.

[37] C. Stähli, M. James-Bhasin, A. Hoppe, A.R. Boccaccini, S.N. Nazhat, Effect of ion release from Cu-doped 45S5 bioglass® on 3D endothelial cell morphogenesis, Acta Biomater. 19 (2015) 15–22, https://doi.org/10.1016/j.actbio.2015.03.009.

[38] U. Gbureck, T. Hölzel, C.J. Doillon, F.A. Müller, J.E. Barralet, Direct printing of bioceramics implants with spatially localized angiogenic factors, Adv. Mater. 19 (2007) 795–800, https://doi.org/10.1002/adma.200601370.

[39] C. Gérard, L.-J. Bordeleau, J. Barralet, C.J. Doillon, The stimulation of angiogenesis and collagen deposition by copper, Biomaterials 31 (2010) 824–831, https://doi.org/10.1016/j.biomaterials.2009.10.009.

[40] S. Gomes, C. Vichery, S. Descamps, H. Martinez, A. Kaur, A. Jacobs, J.M. Nedelec, G. Renaudin, Cu-doping of calcium phosphate bioceramics: from mechanism to the control of cytotoxicity, Acta Biomater. 65 (2018) 462–474, https://doi.org/10.1016/j.actbio.2017.10.028.

[41] L. Yang, S. Perez-Amodio, F.Y.F. Barrère-de Groot, V. Everts, C.A. van Blitterswijk, P. Habibovic, The effects of inorganic additives to calcium phosphate on *in vitro* behavior of osteoblasts and osteoclasts, Biomaterials 31 (2010) 2976–2989, https://doi.org/10.1016/j.biomaterials.2010.01.002.

[42] K. Spaeth, F. Goetz-Neunhoeffer, K. Hurle, Cu2+ doped β-tricalcium phosphate: solid solution limit and crystallographic characterization by rietveld refinement, J. Solid State Chem. 285 (2020) 121225, https://doi.org/10.1016/j.jssc.2020.121225.

[43] P.N. Kumar, M. Boovarasan, R.K. Singh, S. Kannan, Synthesis, structural analysis and fabrication of coatings of the Cu2+ and Sr2+ co-substitutions in β-Ca3(PO4)2, RSC Adv. 3 (2013) 22469, https://doi.org/10.1039/c3ra43171a.

[44] T. Wilson, J.M. Katz, D.H. Gray, Inhibition of active bone resorption by copper, Calcif. Tissue Int. 33 (1981) 35–39, https://doi.org/10.1007/BF02409410.

[45] J. Gallo, S.B. Goodman, Y.T. Konttinen, M.A. Wimmer, M. Holinka, Osteolysis around total knee arthroplasty: a review of pathogenetic mechanisms, Acta Biomater. 9 (2013) 8046–8058, https://doi.org/10.1016/j.actbio.2013.05.005.

[46] B. Le Gars Santoni, L. Niggli, G.A. Sblendorio, D.T.L. Alexander, C. Stähli, P. Bowen, N. Döbelin, M. Bohner, Chemically pure β-tricalcium phosphate powders: evidence of two crystal structures, J. Eur. Ceram. Soc. 41 (2021) 1683–1694, https://doi.org/10.1016/j.jeurceramsoc.2020.09.055.

[47] M. Descamps, J.C. Hornez, A. Leriche, Effects of powder stoichiometry on the sintering of b-tricalcium phosphate, J. Eur. Ceram. Soc. 27 (2007) 2401–2406, https://doi.org/10.1016/j.jeurceramsoc.2006.09.005.

[48] A. Destainville, E. Champion, D. Bernache-Assollant, E. Laborde, Synthesis, characterization and thermal behavior of apatitic tricalcium phosphate, Mater. Chem. Phys. 80 (2003) 269–277, https://doi.org/10.1016/s0254-0584(02)00466-2.

[49] M. Gallo, B. Le Gars Santoni, T. Douillard, F. Zhang, L. Gremillard, S. Dolder, W. Hofstetter, S. Meille, M. Bohner, J. Chevalier, S. Tadier, Effect of grain orientation and magnesium doping on β-tricalcium phosphate resorption behavior, Acta Biomater. 89 (2019) 391–402, https://doi.org/10.1016/j.actbio.2019.02.045.

[50] M. Descamps, O. Richart, P. Hardouin, J.C. Hornez, A. Leriche, Synthesis of macroporous β-tricalcium phosphate with controlled porous architectural, Ceram. Int. 34 (2008) 1131–1137, https://doi.org/10.1016/j.ceramint.2007.01.004.

[51] Implants for Surgery - Hydroxyapatite; Part 3: Chemical Analysis and Characterization of Crystallinity and Phase Purity, 2000.

[52] N. Doebelin, R. Kleeberg, Profex: a graphical user interface for the Rietveld refinement program BGMN, J. Appl. Crystallogr. 48 (2015) 1573–1580, https://doi.org/10.1107/S1600576715014685.

[53] C. Moseke, M. Gelinsky, J. Groll, U. Gbureck, Chemical characterization of hydroxyapatite obtained by wet chemistry in the presence of V, Co, and Cu ions, Mater. Sci. Eng. C 33 (2013) 1654–1661, https://doi.org/10.1016/j.msec.2012.12.075.

[54] K. Poovendran, K.S.J. Wilson, M.S. Revathy, A. Ayeshamariam, K. Kaviyarasu, Functionalization effect of HAp with copper (Cu) having excellent dielectric applications, Surf. Interfaces 19 (2020) 100474, https://doi.org/10.1016/j.surfin.2020.100474.

[55] H. Dai, X. Tan, H. Zhu, T. Sun, X. Wang, Effects of commonly occurring metal ions on hydroxyapatite crystallization for phosphorus recovery from wastewater, Water 10 (2018) 1619, https://doi.org/10.3390/w10111619.

[56] S. Bansal, V. Chauhan, S. Sharma, R. Maheshwari, A. Juyal, S. Raghuvanshi, Evaluation of hydroxyapatite and beta-tricalcium phosphate mixed with bone marrow aspirate as a bone graft substitute for posterolateral spinal fusion, Indian J. Orthop. 43 (2009) 234–239, https://doi.org/10.4103/0019-5413.49387.

[57] T. Suzuki, T. Hatsushika, M. Miyake, Synthetic hydroxyapatites as inorganic cation exchangers. Part 2, Journal of the chemical society, faraday transactions 1, Physical Chemistry in Condensed Phases 78 (1982) 3605–3611, https://doi.org/10.1039/f19827803605.

[58] Y. Takeuchi, H. Arai, Removal of coexisting Pb2+, Cu2+ and Cd2+ ions from water by addition of hydroxyapatite powder, J. Chem. Eng. Japan 23 (1990) 75–80, https://doi.org/10.1252/jcej.23.75.

[59] A. Noori, M. Hoseinpour, S. Kolivand, N. Lotfibakhshaiesh, S. Ebrahimi-Barough, J. Ai, M. Azami, Exploring the various effects of Cu doping in hydroxyapatite nanoparticle, Sci. Rep. 14 (2024) 3421, https://doi.org/10.1038/s41598-024-53704-x.

[60] B. Le Gars Santoni, L. Niggli, S. Dolder, O. Loeffel, G.A. Sblendorio, Y. Maazouz, D. T.L. Alexander, R. Heuberger, C. Stähli, N. Döbelin, P. Bowen, W. Hofstetter, M. Bohner, Influence of the sintering atmosphere on the physico-chemical properties and the osteoclastic resorption of β-tricalcium phosphate cylinders, Acta Biomater. 169 (2023) 566–578, https://doi.org/10.1016/j.actbio.2023.08.012.

[61] L. Vegard, Die Konstitution der Mischkristalle und die Raumfüllung der Atome, Z. Phys. 5 (1921) 17–26, https://doi.org/10.1007/BF01349680.

[62] R. Enderle, F. Gotz-Neunhoeffer, M. Gobbels, F.A. Muller, P. Greil, Influence of magnesium doping on the phase transformation temperature of beta-TCP ceramics examined by Rietveld refinement, Biomaterials 26 (2005) 3379–3384, https://doi.org/10.1016/j.biomaterials.2004.09.017.

[63] S. Gomes, J.-M. Nedelec, E. Jallot, D. Sheptyakov, G. Renaudin, Unexpected mechanism of Zn^{2+} insertion in calcium phosphate bioceramics, Chem. Mater. 23 (2011) 3072–3085, https://doi.org/10.1021/cm200537v.

[64] K. Matsunaga, T. Kubota, K. Toyoura, A. Nakamura, First-principles calculations of divalent substitution of Ca2+ in tricalcium phosphates, Acta Biomater. 23 (2015) 329–337, https://doi.org/10.1016/j.actbio.2015.05.014.

[65] T. Bazin, A. Magnaudeix, R. Mayet, P. Carles, I. Julien, A. Demourgues, M. Gaudon, E. Champion, Sintering and biocompatibility of copper-doped hydroxyapatite bioceramics, Ceram. Int. 47 (2021) 13644–13654, https://doi.org/10.1016/j.ceramint.2021.01.225.

[66] N.V. Bulina, N.V. Eremina, O.B. Vinokurova, A.V. Ishchenko, M.V. Chaikina, Diffusion of copper ions in the lattice of substituted hydroxyapatite during heat treatment, Materials 15 (2022) 5759, https://doi.org/10.3390/ma15165759.

[67] YuO. Nikitina, N.V. Petrakova, A.A. Ashmarin, D.D. Titov, S.V. Shevtsov, T. N. Penkina, E.A. Kuvshinova, S.M. Barinov, V.S. Komlev, N.S. Sergeeva, Preparation and properties of copper-substituted hydroxyapatite powders and ceramics, Inorg. Mater. 55 (2019) 1061–1067, https://doi.org/10.1134/S002016851910011X.

[68] A. Bernhardt, M. Schamel, U. Gbureck, M. Gelinsky, Osteoclastic differentiation and resorption is modulated by bioactive metal ions Co2+, Cu2+ and Cr3+ incorporated into calcium phosphate bone cements, PLoS One 12 (2017) e0182109, https://doi.org/10.1371/journal.pone.0182109.

[69] T.R. Arnett, D.C. Gibbons, J.C. Utting, I.R. Orriss, A. Hoebertz, M. Rosendaal, S. Meghji, Hypoxia is a major stimulator of osteoclast formation and bone resorption, J. Cell. Physiol. 196 (2003) 2–8, https://doi.org/10.1002/jcp.10321.

[70] D.C. Rigiracciolo, A. Scarpelli, R. Lappano, A. Pisano, M.F. Santolla, P. De Marco, F. Cirillo, A.R. Cappello, V. Dolce, A. Belfiore, M. Maggiolini, E.M. De Francesco,

Copper activates HIF-1α/GPER/VEGF signalling in cancer cells, Oncotarget 6 (2015) 34158–34177, https://doi.org/10.18632/oncotarget.5779.
[71] F. Martin, T. Linden, D.M. Katschinski, F. Oehme, I. Flamme, C.K. Mukhopadhyay, K. Eckhardt, J. Tröger, S. Barth, G. Camenisch, R.H. Wenger, Copper-dependent activation of hypoxia-inducible factor (HIF)-1: implications for ceruloplasmin regulation, Blood 105 (2005) 4613–4619, https://doi.org/10.1182/blood-2004-10-3980.
[72] C. Wu, Y. Zhou, M. Xu, P. Han, L. Chen, J. Chang, Y. Xiao, Copper-containing mesoporous bioactive glass scaffolds with multifunctional properties of angiogenesis capacity, osteostimulation and antibacterial activity, Biomaterials 34 (2013) 422–433, https://doi.org/10.1016/j.biomaterials.2012.09.066.
[73] D.A. Palmer, The solubility of crystalline cupric oxide in aqueous solution from 25 °C to 400 °C, J. Chem. Therm. 114 (2017) 122–134, https://doi.org/10.1016/j.jct.2017.03.012.
[74] J. Zhang, J. Huang, S. Xu, K. Wang, S. Yu, Effect of Cu2+ and pH on osteoclastic bone resorption *in vitro*, Prog. Nat. Sci. 13 (2003) 266–270, https://doi.org/10.1080/10020070312331343510.
[75] Appendix B: Solubility-Product Constants (Ksp) for Compounds at 25°C, (n.d.).
[76] I.V. Fadeeva, B.I. Lazoryak, G.A. Davidova, F.F. Murzakhanov, B.F. Gabbasov, N. V. Petrakova, M. Fosca, S.M. Barinov, G. Vadalà, V. Uskoković, Y. Zheng, J.V. Rau, Antibacterial and cell-friendly copper-substituted tricalcium phosphate ceramics for biomedical implant applications, Mater. Sci. Eng. C 129 (2021) 112410, https://doi.org/10.1016/j.msec.2021.112410.
[77] S. Elbashir, R. Salh, B.M. Andersson, New insights into structural and spectroscopic characteristics of Cu2+ doped β-Ca3(PO4)2: correlation between Cu2+ concentration and material properties, Mater. Des. 252 (2025) 113718, https://doi.org/10.1016/j.matdes.2025.113718.